CAPITAL UNIVERSITY OF SCIENCE AND TECHNOLOGY, ISLAMABAD

Effect of Micromagnetorotation on Concentration in a Chemically Reacting Process within Micropolar Boundary Layer

by

Malik Fahad

A thesis submitted in partial fulfillment for the degree of Master of Philosophy

in the

Faculty of Computing

Department of Mathematics

2025

I dedicate my thesis to

my beloved family, friends specially

My Mother(Marjeena Begum),

A determined and aristocratic embodiment who educated me to belief in ALLAH,

believed in hard work and that so much could be done with little,

My Father(Mukhtiar Malik)

I quote the remarkable words of Hadith,

"A father gives his child nothing better than good education."

CERTIFICATE OF APPROVAL

Effect of Micromagnetorotation on Concentration in a Chemically Reacting Process within Micropolar Boundary Layer

by

Malik Fahad

(Registration No: MMT223004)

THESIS EXAMINING COMMITTEE

S. No.	Examiner	Name	Organization
(a)	External Examine	Dr. Saqib Zia	COMSATS, Islamabad
(b)	Internal Examiner	Dr. Muhammad Sagheer	CUST, Islamabad
(c)	Supervisor	Dr. Muhammad Sabeel Khan	CUST, Islamabad

Dr. Muhammad Sabeel Khan
Thesis Supervisor
June, 2025

Dr. Muhammad Sagheer
Head
Dept. of Mathematics
June, 2025

Dr. M. Abdul Qadir
Dean
Faculty of Computing
June, 2025

Author's Declaration

I, **Malik Fahad** hereby state that my MPhil thesis titled "**Effect of Micromagnetorotation on Concentration in a Chemically Reacting Process within Micropolar Boundary Layer**" is my own work and has not been submitted previously by me for taking any degree from Capital University of Science and Technology, Islamabad or anywhere else in the country/abroad.

At any time if my statement is found to be incorrect even after my graduation, the University has the right to withdraw my MPhil Degree.

(Malik Fahad)

Registration No: MMT223004

Plagiarism Undertaking

I solemnly declare that research work presented in this thesis titled "**Effect of Micromagnetorotation on Concentration in a Chemically Reacting Process within Micropolar Boundary Layer**" is solely my research work with no significant contribution from any other person. Small contribution/help wherever taken has been duly acknowledged and that complete thesis has been written by me.

I understand the zero tolerance policy of the HEC and Capital University of Science and Technology towards plagiarism. Therefore, I as an author of the above titled thesis declare that no portion of my thesis has been plagiarized and any material used as reference is properly referred/cited.

I undertake that if I am found guilty of any formal plagiarism in the above titled thesis even after award of MPhil Degree, the University reserves the right to withdraw/revoke my MPhil degree and that HEC and the University have the right to publish my name on the HEC/University website on which names of students are placed who submitted plagiarized work.

(Malik Fahad)

Registration No: MMT223004

Acknowledgement

In the name of **ALLAH**, the Most Merciful and Beneficent, who created the universe and blessed mankind with intelligence and wisdom to explore its secrets. I would like to express my heartfelt gratitude and immeasurable respect to my supervisor, **Dr. Muhammad Sabeel Khan**, for his passionate interest, willingness to help, superb guidance, and inspiration throughout this investigation. His constructive feedback and encouragement greatly helped in shaping this thesis.

I am deeply grateful to all my teachers for their motivation and emphasis on striving for excellence in the pursuit of knowledge. I extend my sincere gratitude to the **Capital University of Science and Technology (CUST)** for providing a supportive environment that greatly facilitated this research.

I owe my deepest gratitude to my father, **Mr. Mukhtiar Malik (Late)**, whose dream has been my guiding light, and my mother, whose prayers have been my greatest strength throughout my life. Their unwavering support and blessings have always inspired me to persevere and achieve my goals.

Finally, I wish to thank my friends and fellow researchers at CUST for their valuable discussions and support during this research. Their camaraderie and insights have enriched my experience, and I am grateful to have shared this journey with them.

(Malik Fahad)
Registration No: MMT223004

Abstract

This study investigates the effect of micromagnetorotation (MMR) on concentration in a chemically reacting process within a micropolar boundary layer. Building upon existing research in magnetohydrodynamic (MHD) micropolar flow, the study integrates mathematical modeling and numerical techniques to examine velocity, temperature, and concentration profiles. Using similarity transformations, the governing partial differential equations (PDEs) are transformed into ordinary differential equations (ODEs) and solved via the shooting method. The results demonstrate that key parameters, including the Prandtl number, Schmidt number, and Reynolds number, significantly influence the flow and thermal characteristics. The study employs mathematical modeling and numerical techniques to analyze micropolar boundary layer flow. Similarity transformations convert PDEs into ODEs, which are then solved using the shooting method with Runge-Kutta integration. The research effectively illustrates how MMR and other parameters impact fluid behavior. The numerical results align with theoretical expectations, particularly regarding the relationships between the Prandtl number and thermal diffusivity. However, the absence of experimental validation raises concerns about the broader applicability of the findings. This study contributes to the growing body of knowledge in MHD and micropolar fluid dynamics, particularly in chemically reacting boundary layers. It offers valuable insights into the interplay between microrotation effects and fluid properties, which could be relevant for industrial applications such as cooling systems, polymer processing, and biomedical engineering.

Contents

List of Figures

List of Tables

Abbreviations

CFD	Computational Fluid Dynamics
FEM	Finite Element Method
IVP	Initial Value Problem
MHD	Magnetohydrodynamics
MMR	Micromagnetorotation
ODEs	Ordinary Differential Equations
PDEs	Partial Differential Equations
RK-4	Runge-Kutta 4

Symbols

κ	Thermal diffusivity
ω	MMR parameter
β^*	Micro-polar coupling parameter
B	Magnetic induction vector
C_f	Skin friction coefficient
C_p	Specific heat
D	Molecular diffusivity
E	Electric field
K	Micropolar parameter
$M \times H$	Micromagnetorotation form
P_r	Prandtl number
Q	Dimensionless heat source
R_e	Reynolds number
S_c	Schmidt number
j	Current density
l	Moment of inertia
p	Pressure
ϕ	Dimensionless concentration
μ_o	Magnetic permeability
$\tilde{\eta}$	Shear viscosity
η_1	Vortex viscosity
ρ	Fluid density
σ	Electrical conductivity
θ	Dimensionless temperature

Chapter 1

Introduction and Literature Survey

The study of fluids dates back to ancient Greece, around 250 BC, when Archimedes formulated the principle of buoyancy, now known as Archimedes' Principle. Fluids are defined as materials or substances that can flow or move.

They are generally categorized into two groups: Newtonian fluids and Non-Newtonian fluids. Boundary layer flows within the framework of the micropolar continuum have been extensively studied due to their significance in various industrial processes. Notable examples include applications such as winding rolls, fluid flow dynamics, metal cooling techniques, continuous filament extrusion in textiles, cable and plastic film production, crystal growth, as well as processes such as in crude oil extraction, food processing, polymer extrusion, and the development of syrup-based medications [1, 2]. The influence of magnetization in the direction lateral to the applied magnetic field is not included in nearly all of the current studies in the literature concerning micropolar boundary layer flows. The magnetization does, however, have an impact on the flow fields laterally [3].

Additionally, Eringen investigated the combined effects of magnetohydrodynamics (MHD) and electrodynamics on micropolar fluids, providing key insights into the complex interactions between magnetic fields and microstructural fluid behavior [4]. Reddy et al. [5] examined the stagnation point flow of MHD nanofluids

over a stretching sheet, emphasizing the influence of magnetic induction on flow characteristics. The micropolar fluid theory is widely utilized in the rheological modeling of complex fluids, including blood, liquid crystals, colloidal suspensions, and non-Newtonian lubricants, as demonstrated in the work of Karvelas et al. [6] examined the flow of blood within a human carotid model, treating blood as a micropolar fluid.Their research focused on the influence of blood microstructure compared to conventional Newtonian fluid behavior. The study revealed that an increase in microrotation and vortex viscosity leads to a significant reduction in wall shear stress. Saraswathy et al. conducted an in-depth investigation into the effects of nonlinear thermal radiation and viscous dissipation in (MHD) micropolar fluid flow through a porous channel, providing valuable insights into the intricate thermal and flow dynamics encountered under such conditions [7]. Their findings highlighted that the microrotation profile exhibits contrasting behavior depending on the spin gradient viscosity and vortex viscosity parameters.

Almakki et al.[8] proposed a micropolar nanofluid model for MHD unsteady flow with entropy generation occurring through a stretched surface at the boundary.The analytical and numerical parts were addressed by Khan and Hackl [9] using relaxation energies. The Cosserat continuum is employed to model materials with microstructures. Within this framework, the interaction energy potential plays a significant role in contributing to the material's free energy, particularly by accounting for the counter-rotational behavior of suspended particles. Similarly, Tulu [10] explored a Cattaneo-Christov model of micropolar MHD nanofluid flow over a radially stretched disk, notably excluding Fickian mass flux and Fourier heat conduction effects. To address the complexities of the nonlinear partial differential equations (PDEs) arising in these studies, the spectral local linearization technique was employed to numerically solve for temperature, concentration, momentum, and microrotation boundary conditions. Khan and Hameed delved into the effects of MHD heat transfer on upper-convected Maxwell micropolar flow, incorporating considerations of thermal radiation and Joule heating. Their research provided critical insights into how microstructural parameters affect microrotations and macroscopic velocity profiles, establishing the angular momentum balance equation with microrotation effects explicitly included. In the context of

a rotating reference frame, Narayana et al. [11] explored the combined effects of radiation absorption and Hall currents on MHD micropolar flow. They further assessed the impact of a magnetic field oriented normal to a porous surface that absorbs micropolar fluid with a uniform suction velocity. Kumar et al. [12] investigated heat generation and absorption phenomena in micropolar MHD flow over a porous medium under the influence of thermal radiation and a magnetic field, incorporating the effects of porous suction and injection.The nonlinear ordinary differential equations (ODEs) arising in their analysis were solved using the shooting method in combination with the fourth-order Runge-Kutta (RK-4) algorithm.

Khan et al. [13] conducted a finite element analysis of MHD micropolar flow through a rectangular channel, utilizing iterative numerical methods to derive their results. They observed that both magnetic induction and the microrotational velocity of particles decrease with an increase in the micropolar coupling parameter. Additionally, Khan and Hameed perform a comprehensive heat transfer analysis within the context of MHD micropolar flow, offering further insights into the complex interactions governing these systems. In 2007, Mahmoud examined how variable thermal conductivity and thermal radiation influence the flow and heat transfer behavior of an electrically conducting micropolar fluid over a continuously stretching surface with a non-uniform temperature, under the influence of a magnetic field. The governing equations were addressed using the shooting technique [14]. In 2014, Mendu analyzed the impact of radiation and chemical reactions on free convection heat and mass transfer in a micropolar fluid, employing the Keller-box method to solve the governing equations. It was found that an increase in the radiation parameter leads to an increase in temperature, velocity, and microrotation profiles [15]. Sagheer et.al investigates the intricate interplay of heat transfer within micropolar magnetohydrodynamic (MHD) flow,emphasizing the role of micromagnetorotation(MMR) by shooting method [16]. The objective of the current analysis is to examine the velocity profile of a steady and incompressible micropolar fluid flow. Additionally, the study incorporates the heat equation and the concentration equation to provide a comprehensive understanding of the system. A brief discussion of the graphical representations of the dimensionless

temperature (θ) and concentration (ϕ) profiles is also included to highlight key findings and physical interpretations.

1.1 Thesis Contribution

The present study extends the model [9] by investigating the effect of micromagnetorotation (MMR) on the concentration within a chemically reacting micropolar boundary layer. Specifically, the study investigates the effects of concentration and energy-related parameters on the velocity, temperature, and concentration distributions, as well as on the skin friction coefficient.

The complex governing non-linear partial differential equations (PDEs) that describe the dynamics of micropolar fluid flow are systematically transformed into a set of dimensionless ordinary differential equations (ODEs) through the application of similarity transformations. This mathematical approach simplifies the problem by reducing the number of independent variables, making the equations more manageable for numerical solutions. To achieve precise and reliable results, the dimensionless ODEs are solved using the shooting method, a robust numerical technique that converts boundary value problems into initial value problems, enhancing the accuracy of the computational process. This thesis culminates with an exhaustive analysis of the numerical results, presented through comprehensive graphical representations. These visualizations offer valuable insights into the influence of critical parameters on the velocity, temperature, and concentration profiles within the flow. The analysis underscores the significant impact of these parameters in defining the behavior and characteristics of chemically reacting micropolar flows, emphasizing their importance in both theoretical modeling and practical applications.

1.2 Thesis Layout

This thesis is further composed of the following chapters:

- **Chapter 2** provides an introduction to the fundamentals of fluid dynamics. It covers essential definitions, the governing laws of fluid motion, and the corresponding equations. Additionally, it briefly discusses dimensionless physical quantities relevant to the problems addressed.

- **Chapter 3** provides an in-depth review of a novel Magneto micropolar boundary layer model for liquid flows, with a particular focus on the effects of micromagnetorotation. This chapter explores the theoretical development of the model, emphasizing its applicability in capturing the intricate dynamics of fluid flows influenced by magnetic fields and micromagnetorotation phenomena. The governing flow equations for this system are solved using the shooting method, a powerful numerical approach for tackling boundary value problems. Detailed numerical results are presented, shedding light on the fluid's behavior under the interplay of micromagnetorotation and magnetohydrodynamic forces. These results are analyzed to uncover critical insights and establish the model's relevance in advancing the understanding of complex fluid mechanics.

- **Chapter 4** builds upon the foundation established in Chapter 3 by extending the analysis of the Magneto micropolar boundary layer model [9]. This extension incorporates the effect of micromagnetorotation on the concentration field within a chemically reactive process. The chapter delves into the interplay between micromagnetorotation and chemical reactions, examining how these interactions influence concentration distribution within the boundary layer. The theoretical framework is expanded to account for additional governing equations that describe the coupled effects of micromagnetorotation and chemical reactivity. Numerical solutions are obtained to analyze these effects in detail, providing insights into the dynamics of concentration profiles under varying magnetic and chemical reaction conditions.

- **Chapter 5** presents the results obtained in Chapter 4 through detailed graphs and tables. These visual and numerical representations highlight the effects of micromagnetorotation on concentration distribution within the chemically reactive micropolar boundary layer. Key trends and comparisons

are analyzed to validate the extended model and its implications for fluid dynamics.

- **Chapter 6** provides the concluding remarks of this thesis, summarizing the key findings and their implications.

Chapter 2

Basic Terminologies

The fundamental concepts, terminologies, and governing principles of fluid dynamics are discussed in this chapter. Additionally, dimensionless quantities, which will be useful in the subsequent chapters, are also introduced.

2.1 Some Basic Definitions

2.1.1 Definition (Fluid)

"A fluid is defined as a substance that undergoes continuous deformation when subjected to any amount of shear (tangential) stress, however small. " [17]

2.1.2 Definition (Fluid Mechanics)

"Fluid mechanics is the branch of science that studies the behavior of fluids (liquids or gases) both at rest and in motion." [18]

2.1.3 Definition (Fluid Dynamics)

"Fluid dynamics is the branch of science that deals with the study of fluids in

motion while considering the effects of pressure forces. " [18]

2.1.4 Definition (Fluid Statics)

"Fluid statics is the study of fluids at rest." [18]

2.1.5 Definition (Viscosity)

"*Viscosity* refers to the property of a fluid that resists the movement of one layer of fluid over another adjacent layer. Mathematically,

$$\mu = \frac{\tau}{\frac{\partial u}{\partial y}}, \tag{2.1}$$

where μ is the viscosity coefficient, τ is the shear stress, and $\frac{\partial u}{\partial y}$ represents the velocity gradient." [18]

2.1.6 Definition (Kinematic Viscosity)

"*Kinematic viscosity* is the ratio of the dynamic viscosity to the density of a fluid. It is denoted by the symbol ν, called *nu*. Mathematically,

$$\nu = \frac{\mu}{\rho}, \tag{2.2}$$

where ν is the kinematic viscosity, μ is the dynamic viscosity, and ρ is the density of the fluid." [18]

2.1.7 Definition (Thermal Conductivity)

"According to Fourier's law of heat conduction, the rate of heat transfer is directly proportional to the temperature gradient. The constant of proportionality is termed the *thermal conductivity*, which may vary depending on different parameters. " [19]

2.1.8 Definition (Thermal Diffusivity)

"The rate at which heat diffuses by conduction through a material depends on the *thermal diffusivity* and can be defined as,

$$\alpha = \frac{k}{\rho C_p}, \tag{2.3}$$

where α is the thermal diffusivity, k is the thermal conductivity, ρ is the density, and C_p is the specific heat at constant pressure." [20]

2.1.9 Definition (Microrotation)

"Microrotation refers to the inherent angular velocity of the particles within a micropolar fluid. In contrast to the macroscopic vorticity of the fluid, microrotation characterizes the rotational behavior of the fluid's microstructure. This rotational motion is represented by the microrotation vector $\boldsymbol{\omega}$, which adheres to governing equations derived from the conservation of angular momentum in the framework of micropolar fluid mechanics.
The microrotation vector $\boldsymbol{\omega}$ is typically linked to the velocity field $\mathbf{u}$ of the fluid through constitutive equations and specific boundary conditions that define the dynamics of micropolar fluids". [21]

2.2 Types of Fluid

2.2.1 Definition (Ideal Fluid)

"A fluid that is incompressible and has no viscosity is called an *ideal fluid*. An ideal fluid is a theoretical concept, as all real fluids have some viscosity." [18]

2.2.2 Definition (Real Fluid)

"A *real fluid* is a fluid that has viscosity. In practice, all fluids are real fluids." [18]

2.2.3 Definition (Newtonian Fluid)

"A *Newtonian fluid* is a real fluid in which the shear stress is directly proportional to the rate of shear strain (or velocity gradient)." [18]

2.2.4 Definition 2.2.4 (Non-Newtonian Fluid)

"A real fluid in which the shear stress is not directly proportional to the rate of shear strain (or velocity gradient) is called a *non-Newtonian fluid*. The relationship between shear stress and velocity gradient for such fluids can be expressed as,

$$\tau_{xy} \propto \left(\frac{du}{dy}\right)^m, \quad m \neq 1 \tag{2.4}$$

or equivalently,

$$\tau_{xy} = \mu \left(\frac{du}{dy}\right)^m, \tag{2.5}$$

where τ_{xy} is the shear stress, $\frac{du}{dy}$ is the rate of shear strain, μ is the viscosity, and m is a constant that is not equal to 1." [18]

2.2.5 Definition (Magnetohydrodynamics)

"*Magnetohydrodynamics (MHD)* studies the interaction between fluid flow and magnetic fields. The fluids considered in this field must be electrically conductive and non-magnetic, typically including liquid metals, hot ionized gases (plasmas), and strong electrolytes." [22]

2.3 Types of flow

2.3.1 Definition (Rotational Flow)

"*Rotational flow* refers to a type of fluid flow in which fluid particles, while moving along streamlines, also rotate about their own axis." [18]

2.3.2 Definition (Irrotational Flow)

"*Irrotational flow* refers to a type of fluid flow in which fluid particles, while moving along streamlines, do not rotate about their own axis." [18]

2.3.3 Definition (Compressible Flow)

"*Compressible flow* is characterized by changes in fluid density at different points. In other words, the density (ρ) of the fluid is not constant. Mathematically,

$$\rho \neq k, \tag{2.6}$$

where k is a constant." [18]

2.3.4 Definition (Incompressible Flow)

"*Incompressible flow* refers to a type of flow where the fluid's density remains constant. Liquids are typically incompressible, whereas gases are generally compressible. Mathematically,

$$\rho = k, \tag{2.7}$$

where k is a constant." [18]

2.3.5 Definition (Steady Flow)

"*Steady flow* occurs when the flow characteristics, such as velocity, depth, or rate of flow, remain constant over time at any given point in an open channel. Mathematically,

$$\frac{\partial Q}{\partial t} = 0, \tag{2.8}$$

where Q represents any fluid property." [18]

2.3.6 Definition (Unsteady Flow)

"*Unsteady flow* refers to a flow condition where the velocity, depth, or rate of flow varies with time at any given point in an open channel. Mathematically."[18]

$$\frac{\partial Q}{\partial t} \neq 0, \tag{2.9}$$

where Q represents any fluid property."

2.3.7 Definition (Internal Flow)

"*Internal flow* describes fluid flow that is entirely confined within solid boundaries, such as in pipes or ducts." [17]

2.3.8 Definition (External Flow)

"*External flow* occurs when a fluid flows around a body that is immersed in an unbounded fluid domain, such as the flow over an aircraft wing or a cylinder." [17]

2.4 Modes of Heat Transfer

2.4.1 Definition (Heat Transfer)

"*Heat transfer* is a field of engineering focused on the movement of thermal energy from one location to another within a medium or between different media due to a temperature difference." [19]

2.4.2 Definition (Conduction)

"*Conduction* refers to the transfer of heat within a material through the process of diffusion." [19]

2.4.3 Definition (Convection)

"*Convection* is the transfer of heat that occurs through energy transport facilitated by fluid motion. Heat transfer between two different media via convection follows Newton's law of cooling." [19]

2.4.4 Definition (Thermal Radiation)

"*Thermal radiation* is radiant energy, in the form of electromagnetic waves, emitted by a medium solely as a result of its temperature." [19]

2.5 Dimensionless Numbers

2.5.1 Definition (Prandtl Number)

"*Prandtl number* is defined as the ratio of momentum diffusivity (ν) to thermal diffusivity (α). It can be expressed as

$$Pr = \frac{\nu}{\alpha} = \frac{\mu}{\rho} \cdot \frac{k}{C_p \rho} = \frac{\mu C_p}{k}, \tag{2.10}$$

where μ is the dynamic viscosity, C_p is the specific heat, and k is the thermal conductivity. The Prandtl number determines the relative thickness of the momentum and thermal boundary layers. When Pr is small, heat is distributed more quickly than momentum." [17]

2.5.2 Definition (Skin Friction Coefficient)

"*Skin friction coefficient* refers to the steady flow of an incompressible fluid, such as a gas or liquid, through a long pipe with a diameter D and a mean velocity u_w. It is given by

$$C_f = \frac{2\tau_0}{\rho u_w^2}, \tag{2.11}$$

where τ_0 represents the wall shear stress and ρ is the density of the fluid."[23]

2.5.3 Definition (Nusselt Number)

"*Nusselt number* is a dimensionless quantity that expresses the ratio of convective to conductive heat transfer across a boundary layer. It is used to characterize the heat transfer from a hot surface to a cold fluid stream, where heat is diffused through the boundary layer and convected away. The Nusselt number is given by

$$Nu = \frac{qL}{k}, \tag{2.12}$$

where q is the convective heat transfer, L is the characteristic length, and k is the thermal conductivity." [24]

2.5.4 Definition (Sherwood Number)

"*Sherwood number* is a dimensionless number that compares the rate of mass transfer by convection to the rate of mass transfer by diffusion. It is mathematically expressed as

$$Sh = \frac{kL}{D}, \tag{2.13}$$

where L is the characteristic length, D is the mass diffusivity, and k is the mass transfer coefficient." [25]

2.5.5 Definition (Reynolds Number)

"*Reynolds number* is a dimensionless number that quantifies the ratio of inertial forces to viscous forces in a flowing fluid. It is defined as

$$Re = \frac{VL}{\nu}, \tag{2.14}$$

where V is the free-stream velocity, L is the characteristic length, and ν is the kinematic viscosity." [18]

2.6 Governing Equations

2.6.1 The Continuity Equation

"*Continuity equation* is derived from the principle of conservation of mass. It states that the time rate of change of mass within a fixed volume is equal to the net rate of mass flow across the surface of that volume. Mathematically, it is expressed as

$$\frac{\partial \rho}{\partial t} + \nabla \cdot (\rho \mathbf{u}) = 0. \tag{2.15}$$

where ρ is the fluid density, and $\mathbf{u}$ is the velocity vector." [19]

2.6.2 The Momentum Equation

"*Momentum equation* states that the time rate of change of linear momentum of a system of particles is equal to the sum of all external forces acting on the particles, considering Newton's third law of action and reaction for the internal forces. Mathematically, it is given by

$$\frac{\partial}{\partial t}(\rho \mathbf{u}) + \nabla \cdot [(\rho \mathbf{u})\mathbf{u}] = \nabla \cdot \mathbf{T} + \rho \mathbf{g}, \tag{2.16}$$

where $\mathbf{T}$ is the stress tensor and $\mathbf{g}$ is the gravitational force." [19]

2.6.3 The Energy Equation

"*Energy equation* is based on the law of conservation of energy. It states that the time rate of change of the total energy is equal to the sum of the rate of work done by external forces, the change in heat content, and the dissipation of energy. The energy equation is mathematically written as

$$\frac{\partial \rho}{\partial t} + \nabla \cdot \rho \mathbf{u} = -\nabla \cdot \mathbf{q} + Q + \phi, \tag{2.17}$$

where $\mathbf{q}$ is the heat flux, Q is the heat source, and ϕ is the dissipation function." [19]

2.7 Shooting Method

The shooting method is a popular numerical technique used to solve higher-order nonlinear ordinary differential equations (ODEs) with specified boundary conditions. The fundamental approach involves transforming the given higher-order ODEs into an equivalent system of first-order ODEs. This transformation simplifies the problem by expressing it as a system of equations that can be handled more efficiently using numerical integration methods.

Once the system is established, the next step is to address the issue of missing initial conditions. Since boundary value problems often involve conditions specified at multiple points rather than a single initial point, an appropriate set of initial conditions must be assumed to begin the numerical integration. These assumed values are crucial in ensuring that the solution aligns with the given boundary conditions. The resulting system of first-order ODEs, together with the assumed initial conditions, is treated as an initial value problem and solved using a numerical integration method—typically the Runge-Kutta method, known for its accuracy in iterative solutions over a specified interval. The computed solution at the endpoint is then evaluated against the given boundary conditions to assess its validity. To achieve the desired accuracy, an iterative refinement process is applied. If the calculated values at the terminal point deviate from the given boundary conditions beyond an acceptable threshold, the assumed initial conditions are adjusted accordingly. This adjustment is carried out using Newton's method, which is an efficient root-finding technique that iteratively refines the values until the boundary conditions are satisfied within the required precision. This iterative process continues until a satisfactory solution is obtained, ensuring that the numerical integration yields results that accurately satisfy the boundary constraints of the original higher-order nonlinear ODEs.

To elaborate on the shooting method, consider the following nonlinear boundary value problem:

$$f''(x) = f(x)f'(x) + 2f^2(x), \tag{2.18}$$

subject to the boundary conditions:

$$f(0) = 0, \quad f(G) = J. \tag{2.19}$$

2.7.1 Reduction to First-Order ODEs

Introduce the following substitutions:

$$f = Z_1, \quad f' = Z_2, \quad f'' = Z_2', \tag{2.20}$$

which convert the boundary value problem into the following system of first-order ODEs:

$$Z_1' = Z_2, \quad Z_1(0) = 0, \tag{2.21}$$

$$Z_2' = Z_1 Z_2 + 2Z_1^2, \quad Z_2(0) = v, \tag{2.22}$$

where v is the unknown initial condition.

2.7.2 Numerical Solution Using RK-4 Method

Solve the above initial value problem (IVP) using the fourth-order Runge-Kutta (RK-4) method. Adjust v such that:

$$Z_1(H, v) = K. \tag{2.23}$$

Let $Z_1(H, v)$ be denoted as $Z_1(v)$, and define:

$$F(v) = Z_1(v) - K. \tag{2.24}$$

Newton's method is applied to solve $F(v) = 0$ using the iterative formula:

$$v_{n+1} = v_n - \frac{F(v_n)}{F'(v_n)}, \tag{2.25}$$

or equivalently:

$$v_{n+1} = v_n - \frac{Z_1(v_n) - K}{\frac{\partial Z_1(v_n)}{\partial v}}. \tag{2.26}$$

2.7.3 Deriving the Derivatives

Introduce the following substitutions:

$$\frac{dZ_1}{dv} = Z_3, \quad \frac{dZ_2}{dv} = Z_4. \tag{2.27}$$

The Newton iteration becomes:

$$v_{n+1} = v_n - \frac{Z_1(v_n) - K}{Z_3(v_n)}. \tag{2.28}$$

2.7.4 Extended System of ODEs

Differentiating the original system with respect to v, we obtain the extended system:

$$Z_1' = Z_2, \qquad Z_1(0) = 0, \tag{2.30}$$

$$Z_2' = Z_1 Z_2 + 2Z_1^2, \qquad Z_2(0) = v, \tag{2.31}$$

$$Z_3' = Z_4, \qquad Z_3(0) = 0, \tag{2.32}$$

$$Z_4' = Z_3 Z_2 + Z_1 Z_4 + 4Z_1 Z_3, \qquad Z_4(0) = 1. \tag{2.33}$$

2.7.5 Stopping Criterion

The iteration halts when:

$$|Z_1(v) - K| < \epsilon, \tag{2.29}$$

where $\epsilon > 0$ is a predefined tolerance.

Chapter 3

A Magneto-Micropolar Boundary Layer Model for Liquid Flows with Micromagnetorotation Effects

3.1 Introduction

In this chapter, a numerical study is conducted on magnetohydrodynamic (MHD) convection within micropolar fluids under the influence of an external magnetic field. The nonlinear partial differential equations (PDEs) governing the flow are transformed into ordinary differential equations (ODEs) using similarity variables. These resulting ODEs are solved using the shooting method in MATLAB. The results are presented graphically to highlight the key physical insights and trends.

3.2 Physical Model

The study investigates the two-dimensional flow of a micropolar fluid influenced by magnetohydrodynamic (MHD) convection in the presence of an externally imposed

magnetic field. The Cartesian coordinate system is aligned so that the x-axis corresponds to the direction of the free stream flow, while the y-axis is oriented normal to the surface. This configuration gives rise to the development of boundary layers related to velocity, temperature, concentration and micro-polar fields. The physical setup along with the coordinate system is depicted in the figure.

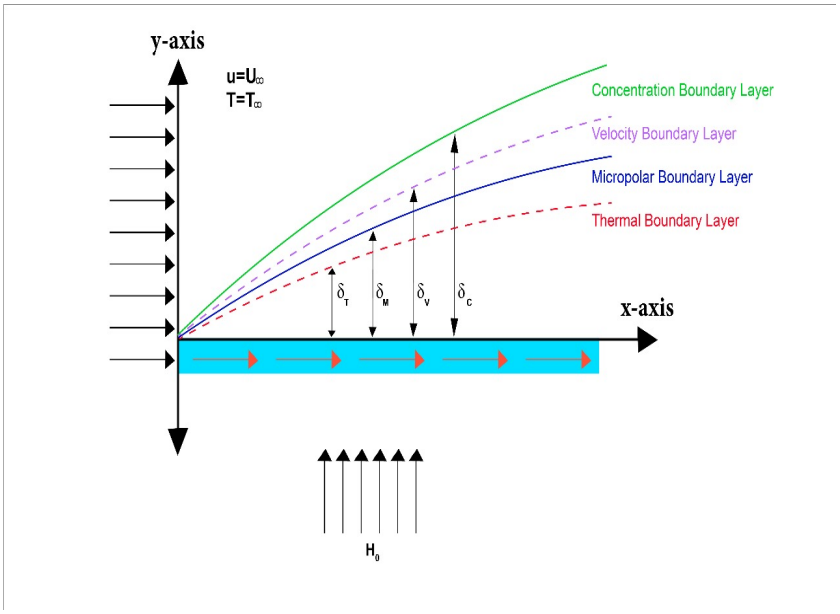

FIGURE 3.1: Geometric description of the model

The vector form of the governing equations is as follow:

$$\nabla \cdot \mathbf{U} = 0, \tag{3.1}$$

$$\nabla \cdot \mathbf{H} = 0, \tag{3.2}$$

$$\begin{aligned} \rho\frac{d\mathbf{U}}{dt} + \mathbf{U}\cdot\nabla\mathbf{U} + \nabla p = \tilde{\eta}\nabla^2\mathbf{U} + 2\eta_1\nabla\times(\mathbf{W}-\mathbf{w}) \\ + (\nabla\times\mathbf{H})\times\mathbf{B} + (\mathbf{M}\cdot\nabla)\mathbf{H} + \mathbf{M}\times(\nabla\times\mathbf{H}) \end{aligned} \tag{3.3}$$

$$\rho\frac{d\mathbf{H}}{dt} + \mathbf{U}\cdot\nabla\mathbf{H} = \tilde{\eta}\nabla^2\mathbf{H} + \mathbf{H}\cdot\nabla\mathbf{U}, \tag{3.4}$$

$$l\frac{d\mathbf{W}}{dt} = \gamma\nabla^2\mathbf{W} + 4\eta_1(\mathbf{w}-\mathbf{W}) + \mathbf{M}\times\mathbf{H} - \mathbf{U}\cdot\nabla\mathbf{W}, \tag{3.5}$$

$$\mathbf{B} - \mathbf{M} = \mu_0\mathbf{H}, \tag{3.6}$$

$$\mathbf{M}\cdot\frac{\bar{H}}{\mathbf{H}} = M_0(\mathbf{I} - \tau\mathbf{W}\cdot\boldsymbol{\epsilon}), \tag{3.7}$$

$$\mathbf{J} = \nabla \times \mathbf{H}, \tag{3.8}$$

$$\mathbf{J} = \sigma \left(\mathbf{E} + \mathbf{U} \times \mathbf{B} \right). \tag{3.9}$$

In this context, the variables are defined as,

ρ denotes the fluid density,

p represents the pressure,

$\mathbf{j}$ is the current density,

l is the moment of inertia,

μ_0 is the magnetic permeability,

σ is the electrical conductivity,

$\mathbf{B}$ refers to the magnetic induction vector,

η is the shear viscosity,

η_1 is the vortex viscosity,

γ is the angular viscosity,

$\mathbf{M} \times \mathbf{H}$ describes the MMR effect,

which accounts for how magnetization influences microrotation.

3.3 Governing Equations in The Operator Form

In this section, the process of transforming the governing equations from their vector form to the operator form is presented. The vector form expresses the fundamental principles governing the system in an abstract mathematical framework, whereas the operator form provides a more explicit representation in terms of physical variables and parameters, making the equations more suitable for further analytical or numerical treatment.

3.3.1 Continuity Equation

$$\nabla \cdot \mathbf{U} = 0 \tag{3.10}$$

$$\left(\frac{\partial}{\partial x}, \frac{\partial}{\partial y}, 0\right) \cdot (u, v, 0) = 0 \tag{3.11}$$

$$\Rightarrow \frac{\partial u}{\partial x} + \frac{\partial v}{\partial y} = 0 \tag{3.12}$$

$$\nabla \cdot \mathbf{H} = 0 \tag{3.13}$$

$$\Rightarrow \frac{\partial H_1}{\partial x} + \frac{\partial H_2}{\partial y} = 0 \tag{3.14}$$

3.3.2 Momentum Equation

$$\mathbf{U} \cdot \nabla \mathbf{U} = (u, v, 0) \cdot \left(\frac{\partial}{\partial x}, \frac{\partial}{\partial y}, 0\right)(u, v, 0) \tag{3.15}$$

$$= u\frac{\partial}{\partial x}(u, v, 0) + v\frac{\partial}{\partial y}(u, v, 0) \tag{3.16}$$

$$= \left(u\frac{\partial u}{\partial x} + v\frac{\partial u}{\partial y}, u\frac{\partial v}{\partial x} + v\frac{\partial v}{\partial y}, 0\right) \tag{3.17}$$

Laplacian of Velocity

$$\nabla^2 \mathbf{U} = \left(\frac{\partial^2 u}{\partial x^2} + \frac{\partial^2 u}{\partial y^2}, \frac{\partial^2 v}{\partial x^2} + \frac{\partial^2 v}{\partial y^2}, 0\right) \tag{3.18}$$

Curl Terms

$$2\eta_1 \nabla \times (\mathbf{W} - \mathbf{w}) = 2\eta_1(\nabla \times \mathbf{W}) - 2\eta_1(\nabla \times \mathbf{w})$$

$$= 2\eta_1(\nabla \times \mathbf{W}) - 2\eta_1 \left(\nabla \times \left(\nabla \times \frac{\mathbf{U}}{2}\right)\right) \tag{3.19}$$

Curl of $\mathbf{W} = (0, 0, N)$

$$\nabla \times \mathbf{W} = \begin{vmatrix} \hat{i} & \hat{j} & \hat{k} \\ \frac{\partial}{\partial x} & \frac{\partial}{\partial y} & 0 \\ 0 & 0 & N \end{vmatrix} = \left(\frac{\partial N}{\partial y}, -\frac{\partial N}{\partial x}, 0 \right) \tag{3.20}$$

Curl of U

$$\nabla \times \mathbf{U} = \begin{vmatrix} \hat{i} & \hat{j} & \hat{k} \\ \frac{\partial}{\partial x} & \frac{\partial}{\partial y} & 0 \\ u & v & 0 \end{vmatrix} = \left(0, 0, \frac{\partial v}{\partial x} - \frac{\partial u}{\partial y} \right) \tag{3.21}$$

Curl of Curl of U

$$\begin{aligned} \nabla \times (\nabla \times \mathbf{U}) &= \begin{vmatrix} \hat{i} & \hat{j} & \hat{k} \\ \frac{\partial}{\partial x} & \frac{\partial}{\partial y} & 0 \\ 0 & 0 & \frac{\partial v}{\partial x} - \frac{\partial u}{\partial y} \end{vmatrix} \\ &= \left(\frac{\partial^2 v}{\partial y \partial x} - \frac{\partial^2 u}{\partial y^2}, -\left(\frac{\partial^2 v}{\partial x^2} - \frac{\partial^2 u}{\partial x \partial y} \right), 0 \right) \end{aligned} \tag{3.22}$$

$$\mathbf{J} \times \mathbf{B} = \sigma \left(\mathbf{E} + \mathbf{U} \times \mathbf{B} \right) \times \mathbf{B} \approx \sigma (\mathbf{U} \times \mathbf{B}) \times \mathbf{B}. \tag{3.23}$$

$$\mathbf{U} \times \mathbf{B} = \mu_0 \begin{vmatrix} \hat{i} & \hat{j} & \hat{k} \\ u & v & 0 \\ H_1 + M_0 & H_2 - \tau M_0 N & 0 \end{vmatrix} = \mu_0 \left(u H_2 - u \tau M_0 N - v H_1 - v M_0 \right) \hat{k}.$$

$$(\mathbf{U} \times \mathbf{B}) \times \mathbf{B} = \mu_0 \begin{vmatrix} \mathbf{i} & \mathbf{j} & \mathbf{k} \\ 0 & 0 & u H_2 - u \tau M_0 N - v H_1 - v M_0 \\ H_1 + M_0 & H_2 - \tau M_0 N & 0 \end{vmatrix}$$

$$= \mu_0\Big[\big(- uH_2^2 - uH_2\tau M_0 N - vM_0H_2 + uH_2\tau M_0 N + u\tau^2 M_0^2 N^2$$
$$+ vH_1\tau M_0 N + v\tau M_0^2 N\big)\mathbf{i}$$

$$-\big(uH_2H_1 + uH_2\tau M_0 N + vH_1^2 + vM_0H_1 + uH_2M_0 + u\tau M_0^2 N\big)\mathbf{j} + 0\cdot\mathbf{k}\Big]$$

$$\begin{aligned} = \sigma\mu_0\Big[&\big(- uH_2^2 - vH_1H_2 - vM_0H_2 + u\tau^2M_0^2N^2 + vH_1\tau M_0N + v\tau M_0^2N\big), \\ &\big(uH_2H_1 + uH_2\tau M_0N + vH_1^2 + vM_0H_1 + uH_2M_0 \\ &\quad + u\tau M_0^2N + vH_1M_0 + vM_0^2\big) \\ &0\Big]. \end{aligned} \tag{3.24}$$

$$\begin{aligned} (\mathbf{M}.\boldsymbol{\nabla})\mathbf{H} &= \left(M_0\frac{(H_1+\tau H_2N)}{H_1}, M_0\frac{(H_2-\tau H_1N)}{H_2}, 0\right).\left(\frac{\partial}{\partial x}, \frac{\partial}{\partial y}, 0\right)(H_1, H_2, 0), \\ &= \left(M_0\frac{(H_1+\tau H_2N)}{H_1}\frac{\partial}{\partial x} + M_0\frac{(H_2-\tau H_1N)}{H_2}\frac{\partial}{\partial y} + 0\right)(H_1, H_2, 0), \\ &= M_0\frac{(H_1+\tau H_2N)}{H_1}\frac{\partial}{\partial x}(H_1, H_2, 0) + M_0\frac{(H_2-\tau H_1N)}{H_2}\frac{\partial}{\partial y}(H_1, H_2, 0) \\ &\quad + 0(H_1, H_2, 0) \end{aligned}$$

$$\begin{aligned} &= \left(M_0\frac{H_1+\tau H_2N}{H_1}\frac{\partial H_1}{\partial x},\ M_0\frac{H_1+\tau H_2N}{H_1}\frac{\partial H_2}{\partial x},\ 0\right) \\ &\quad + \left(M_0\frac{H_2-\tau H_1N}{H_2}\frac{\partial H_1}{\partial y},\ M_0\frac{H_2-\tau H_1N}{H_2}\frac{\partial H_2}{\partial y},\ 0\right), \\ &= \left(M_0\frac{H_1+\tau H_2N}{H_1}\frac{\partial H_1}{\partial x} + M_0\frac{H_2-\tau H_1N}{H_2}\frac{\partial H_1}{\partial y},\right. \\ &\qquad \left. M_0\frac{H_1+\tau H_2N}{H_1}\frac{\partial H_2}{\partial x} + M_0\frac{H_2-\tau H_1N}{H_2}\frac{\partial H_2}{\partial y},\ 0\right). \end{aligned} \tag{3.25}$$

Now, the cross product $\mathbf{M} \times (\boldsymbol{\nabla} \times \mathbf{H})$ is computed as follows:

$$\boldsymbol{\nabla} \times \mathbf{H} = \begin{vmatrix} \hat{i} & \hat{j} & \hat{k} \\ \frac{\partial}{\partial x} & \frac{\partial}{\partial y} & 0 \\ H_1 & H_2 & 0 \end{vmatrix}$$

$$= (0)\hat{i} - (0)\hat{j} + \left(\frac{\partial H_2}{\partial x} - \frac{\partial H_1}{\partial y}\right)\hat{k}.$$

$$\mathbf{M} \times (\boldsymbol{\nabla} \times \mathbf{H}) = \begin{vmatrix} \hat{i} & \hat{j} & \hat{k} \\ M_0\frac{(H_1+\tau H_2 N)}{H_1} & M_0\frac{(H_2-\tau H_1 N)}{H_2} & 0 \\ 0 & 0 & \frac{\partial H_2}{\partial x} - \frac{\partial H_1}{\partial y} \end{vmatrix}$$

$$= \left(M_0\frac{(H_2 - \tau H_1 N)}{H_2}\frac{\partial H_2}{\partial x} - M_0\frac{(H_2 - \tau H_1 N)}{H_2}\frac{\partial H_1}{\partial y}\hat{i}\right.$$

$$- M_0\frac{(H_1 + \tau H_2 N)}{H_1}\frac{\partial H_2}{\partial x} + M_0\frac{(H_1 + \tau H_2 N)}{H_1}\frac{\partial H_1}{\partial y}\hat{j}$$

$$\left. + 0\hat{k}\right). \tag{3.26}$$

Now, we substitute all the expressions (3.17)-(3.26) into equation (3.3) to get the following:

$$\rho\left(\frac{du}{dt}, \frac{dv}{dt}, 0\right) + \left(u\frac{\partial u}{\partial x} + v\frac{\partial u}{\partial y}, u\frac{\partial v}{\partial x} + v\frac{\partial v}{\partial y}, 0\right)$$

$$= -\left(\frac{\partial p}{\partial x}, \frac{\partial p}{\partial y}, 0\right) + \mu\left(\frac{\partial^2 u}{\partial x^2} + \frac{\partial^2 u}{\partial y^2}, \frac{\partial^2 v}{\partial x^2} + \frac{\partial^2 v}{\partial y^2}, 0\right)$$

$$+ 2\zeta_1\left(\frac{\partial N}{\partial y} - \frac{\partial N}{\partial x}, 0\right) - \zeta_1\left(\frac{\partial^2 v}{\partial y \partial x} - \frac{\partial^2 u}{\partial y^2}, -\frac{\partial^2 v}{\partial x^2} - \frac{\partial^2 u}{\partial x \partial y}, 0\right)$$

$$+ \sigma\mu_0(-uH_2^2 - vH_1H_2 - vM_0H_2 + u\tau^2M_0^2N^2 + vH_1\tau M_0N$$

$$+ v\tau M_0^2 N, uH_2H_1 + uH_2\tau M_0N + vH_1^2 + vM_0H_1$$

$$+ uH_2M_0 + u\tau M_0^2N + vH_1M_0 + vM_0^2, 0)$$

$$\left(M_0\frac{(H_1+\tau H_2N)}{H_1}\frac{\partial H_1}{\partial x}+M_0\frac{(H_2-\tau H_1N)}{H_2}\frac{\partial H_1}{\partial y},\right.$$
$$\left.M_0\frac{(H_1+\tau H_2N)}{H_1}\frac{\partial H_2}{\partial x}+M_0\frac{(H_2-\tau H_1N)}{H_2}\frac{\partial H_2}{\partial y},0\right)$$
$$+\left(M_0\frac{(H_2-\tau H_1N)}{H_2}\frac{\partial H_2}{\partial x}-M_0\frac{(H_2-\tau H_1N)}{H_2}\frac{\partial H_1}{\partial y},\right.$$
$$\left.-M_0\frac{(H_1+\tau H_2N)}{H_1}\frac{\partial H_2}{\partial x}+M_0\frac{(H_1+\tau H_2N)}{H_1}\frac{\partial H_1}{\partial y},0\right).$$

$$\Rightarrow\quad \frac{du}{dt}+\left(u\frac{\partial u}{\partial x}+v\frac{\partial u}{\partial y}\right)=-\frac{1}{\rho}.\frac{\partial p}{\partial x}+\frac{\mu}{\rho}\left(\frac{\partial^2u}{\partial x^2}+\frac{\partial^2u}{\partial y^2}\right)+\frac{2\zeta_1}{\rho}\left(\frac{\partial N}{\partial y}\right)$$
$$-\frac{k}{\rho}\left(\frac{\partial^2v}{\partial y\partial x}-\frac{\partial^2u}{\partial y^2}\right)+\frac{\sigma}{\rho}\mu_0(-uH_2^2)$$
$$+\frac{1}{\rho}M_0\frac{(H_1+\tau H_2N)}{H_1}\frac{\partial H_1}{\partial x}+M_0\frac{(H_2-\tau H_1N)}{H_2}\frac{\partial H_1}{\partial y}$$
$$+M_0\frac{(H_2-\tau H_1N)}{H_2}\frac{\partial H_2}{\partial x}-M_0\frac{(H_2-\tau H_1N)}{H_2}\frac{\partial H_1}{\partial y}.$$

$$\Rightarrow\quad u\frac{\partial u}{\partial x}+v\frac{\partial u}{\partial y}=\left(\frac{\mu+k}{\rho}\right)\frac{\partial^2u}{\partial y^2}-\frac{\sigma}{\rho}\mu_0H_2^2u+\frac{2k}{\rho}\frac{\partial N}{\partial y}$$
$$+\frac{1}{\rho}\frac{M_0}{\bar{H}}(H_1+\tau H_2N)\frac{\partial H_1}{\partial x}+(H_2-\tau H_1N)\frac{\partial H_2}{\partial x}. \tag{3.27}$$

3.3.3 Magnetic Induction Equation

$$\mathbf{U}\cdot\nabla\mathbf{H}=(u,v,0)\cdot\left(\frac{\partial}{\partial x},\frac{\partial}{\partial y},0\right)(H_1,H_2,0)$$
$$=\left(u\frac{\partial}{\partial x}+v\frac{\partial}{\partial y}\right)(H_1,H_2,0)$$
$$=u\frac{\partial}{\partial x}(H_1,H_2,0)+v\frac{\partial}{\partial y}(H_1,H_2,0)$$
$$=\left(u\frac{\partial H_1}{\partial x},u\frac{\partial H_2}{\partial x},0\right)+\left(v\frac{\partial H_1}{\partial y},v\frac{\partial H_2}{\partial y},0\right)$$
$$=\left(u\frac{\partial H_1}{\partial x}+v\frac{\partial H_1}{\partial y}+u\frac{\partial H_2}{\partial x}+v\frac{\partial H_2}{\partial y},0\right). \tag{3.28}$$

$$\mathbf{H}\cdot\nabla\mathbf{U}=(H_1,H_2,0)\cdot\left(\frac{\partial}{\partial x},\frac{\partial}{\partial y},0\right)(u,v,0)$$
$$=(H_1\frac{\partial}{\partial x},H_2\frac{\partial}{\partial y},0)(u,v,0)$$

$$= H_1 \frac{\partial}{\partial x}(u, v, 0) + H_2 \frac{\partial}{\partial y}(u, v, 0)$$

$$= \left(H_1 \frac{\partial u}{\partial x}, H_1 \frac{\partial v}{\partial x} \right) + \left(H_2 \frac{\partial u}{\partial y}, H_2 \frac{\partial v}{\partial y} \right)$$

$$= \left(H_1 \frac{\partial u}{\partial x} + H_2 \frac{\partial u}{\partial y}, H_1 \frac{\partial v}{\partial x} + H_2 \frac{\partial v}{\partial y}, 0 \right). \tag{3.29}$$

$$\nabla^2 \mathbf{H} = \left(\tfrac{\partial}{\partial x}, \tfrac{\partial}{\partial y}, 0 \right) \left(\tfrac{\partial}{\partial x}, \tfrac{\partial}{\partial y}, 0 \right) (H_1, H_2, 0)$$

$$= \left(\frac{\partial^2}{\partial x^2} + \frac{\partial^2}{\partial y^2} \right) (H_1, H_2, 0)$$

$$= \left(\frac{\partial^2 H_1}{\partial x^2}, \frac{\partial^2 H_2}{\partial x^2}, 0 \right) + \left(\frac{\partial^2 H_1}{\partial y^2}, \frac{\partial^2 H_2}{\partial y^2}, 0 \right)$$

$$= \left(\frac{\partial^2 H_1}{\partial x^2} + \frac{\partial^2 H_1}{\partial y^2}, \frac{\partial^2 H_2}{\partial x^2} + \frac{\partial^2 H_2}{\partial y^2}, 0 \right). \tag{3.30}$$

Now, we put all expressions (3.28)–(3.30) into equation (3.4) to get the following:

$$\begin{aligned} \rho \left(\frac{dH_1}{dt}, \frac{dH_2}{dt}, 0 \right) + \left(u \frac{\partial H_1}{\partial x} + v \frac{\partial H_1}{\partial y}, u \frac{\partial H_2}{\partial x} + v \frac{\partial H_2}{\partial y}, 0 \right) \\ - \left(H_1 \frac{\partial v}{\partial x} + H_2 \frac{\partial u}{\partial y}, H_1 \frac{\partial v}{\partial x} + H_2 \frac{\partial u}{\partial y}, 0 \right) \\ = \mu_0 \left(\frac{\partial^2 H_1}{\partial x^2} + \frac{\partial^2 H_1}{\partial y^2}, \frac{\partial^2 H_2}{\partial x^2} + \frac{\partial^2 H_2}{\partial y^2}, 0 \right) \end{aligned}$$

$$\Rightarrow \frac{dH_1}{dt} + \left(u \frac{\partial H_1}{\partial x} + v \frac{\partial H_1}{\partial y} \right) - \left(H_1 \frac{\partial v}{\partial x} + H_2 \frac{\partial u}{\partial y} \right) = \frac{\mu_0}{\rho} \left(\frac{\partial^2 H_1}{\partial x^2} + \frac{\partial^2 H_1}{\partial y^2} \right)$$

$$\Rightarrow u \frac{\partial H_1}{\partial x} + v \frac{\partial H_1}{\partial y} = H_1 \frac{\partial v}{\partial x} + H_2 \frac{\partial u}{\partial y} + \nu_0 \left(\frac{\partial^2 H_1}{\partial y^2} \right). \tag{3.31}$$

3.3.4 Microrotation Equation

$$\begin{aligned}
\mathbf{U}\cdot\nabla\mathbf{W} &= (u,v,0)\cdot\left(\frac{\partial}{\partial x}\frac{\partial}{\partial y},0\right)(0,0,N)\\
&= \left(u\frac{\partial}{\partial x}+v\frac{\partial}{\partial y}+0\right)(0,0,N)\\
&= u\frac{\partial}{\partial x}(0,0,N)+v\frac{\partial}{\partial y}(0,0,N)+0(0,0,N)\\
&= \left(\frac{\partial(0)}{\partial x},\frac{\partial(0)}{\partial x},\frac{\partial N}{\partial x}\right)u+\left(\frac{\partial(0)}{\partial y},\frac{\partial(0)}{\partial y},\frac{\partial N}{\partial y}\right)v+(0)\\
&= \left(0,0,u\frac{\partial N}{\partial x}\right)+\left(0,0,v\frac{\partial N}{\partial y}\right)+(0)\\
&= \left(0,0,u\frac{\partial N}{\partial x}+v\frac{\partial N}{\partial y}\right). \qquad (3.32)
\end{aligned}$$

$$\begin{aligned}
\gamma\nabla^2\mathbf{W} &= \gamma\left(\frac{\partial^2}{\partial x^2}+\frac{\partial^2}{\partial y^2},0\right)(0,0,N)\\
&= \gamma\left(\frac{\partial^2}{\partial x^2}+\frac{\partial^2}{\partial y^2}\right)(0,0,N)\\
&= \gamma\left(\frac{\partial^2}{\partial x^2}(0,0,N)+\frac{\partial^2}{\partial y^2}(0,0,N)\right)\\
&= \gamma\left(0,0,\frac{\partial^2 N}{\partial x^2}+\frac{\partial^2 N}{\partial y^2}\right). \qquad (3.33)
\end{aligned}$$

$$\begin{aligned}
4\eta_1(\mathbf{w}-\mathbf{W}) &= 4\eta_1\mathbf{w}-4\eta_1\mathbf{W}\\
&= 4\eta_1\left(\nabla\times\frac{\mathbf{U}}{2}\right)-4\eta_1\mathbf{W}, \quad \text{(using (3.7))}\\
&= 2\eta_1\left(\nabla\times\mathbf{U}-2\mathbf{W}\right).
\end{aligned}$$

$$\nabla\times\mathbf{U} = \begin{vmatrix} \hat{i} & \hat{j} & \hat{k}\\ \frac{\partial}{\partial x} & \frac{\partial}{\partial y} & 0\\ u & v & 0 \end{vmatrix} = (0)\hat{i}-(0)\hat{j}+\left(\frac{\partial v}{\partial x}-\frac{\partial u}{\partial y}\right)\hat{k},$$

$$\begin{aligned}
&= 2\eta_1\left(0,0,\frac{\partial v}{\partial x}-\frac{\partial u}{\partial y}\right)-4\eta_1(0,0,N)\\
&= 2\eta_1\left(0,0,\frac{\partial v}{\partial x}-\frac{\partial u}{\partial y}-2N\right). \qquad (3.34)
\end{aligned}$$

The cross product $\mathbf{M} \times \mathbf{H}$ is :

$$\begin{aligned}\mathbf{M} \times \mathbf{H} &= \begin{vmatrix} \hat{i} & \hat{j} & \hat{k} \\ M_0 & -\tau M_0 N & 0 \\ H_1 & H_2 & 0 \end{vmatrix} \\ &= \left(M_0 H_2 - (-\tau M_0 N) H_1\right) \hat{k} \\ &= M_0 \left(H_2 + \tau H_1 N\right) \hat{k}. \end{aligned} \tag{3.35}$$

We substitute all the expressions (3.32)-(3.35) into(3.5), to get:

$$\begin{aligned} l\left(0,0,\frac{dN}{dt}+0,0,u\frac{\partial N}{\partial y}+v\frac{\partial N}{\partial y}\right) &= \gamma\left(0,0,\frac{\partial^2 N}{\partial x^2}+\frac{\partial^2 N}{\partial y^2}\right) \\ &\quad + 2\eta_1\left(0,0,\frac{\partial v}{\partial x}-\frac{\partial u}{\partial y}-0,0,2N\right) \\ &\quad + (0,0,M_0H_2+M_0\tau H_1 N). \end{aligned}$$

$$\begin{aligned} \Rightarrow \quad \left(0,0,\frac{dN}{dt}+0,0,u\frac{\partial N}{\partial x}+v\frac{\partial N}{\partial y}\right) &= \frac{\gamma}{l}\left(0,0,\frac{\partial^2 N}{\partial x^2}+\frac{\partial^2 N}{\partial y^2}\right) \\ &\quad + \frac{2\eta_1}{l}\left(0,0,\frac{\partial v}{\partial x}-\frac{\partial u}{\partial y}-0,0,2N\right) \\ &\quad + \frac{1}{l}(0,0,M_0H_2-M_0\tau H_1 N). \end{aligned}$$

$$\Rightarrow \quad u\frac{\partial N}{\partial x}+v\frac{\partial N}{\partial y}=\frac{\gamma}{l}\frac{\partial^2 N}{\partial y^2}-\frac{2\eta_1}{l}\left(2N+\frac{\partial u}{\partial y}\right)-\frac{1}{l}M_0\tau\bar{H}N. \tag{3.36}$$

The component form of governing equations:

$$\frac{\partial u}{\partial x}+\frac{\partial v}{\partial y}=0. \tag{3.37}$$

$$\frac{\partial H_1}{\partial x}+\frac{\partial H_2}{\partial y}=0. \tag{3.38}$$

$$\begin{aligned} u\frac{\partial u}{\partial x}+v\frac{\partial u}{\partial y} &= (\mu+k)\frac{1}{\rho}\frac{\partial^2 u}{\partial y^2}-\frac{\sigma}{\rho}\mu_0 H_2^2 u+\frac{k}{\rho}\frac{\partial N}{\partial y} \\ &\quad + \frac{1}{\rho M_0\bar{H}}\left(H_1+\tau N H_2\right)\frac{\partial H_1}{\partial x}+\left(H_2-\tau N H_1\right)\frac{\partial H_2}{\partial x}. \end{aligned} \tag{3.39}$$

$$u\frac{\partial H_1}{\partial x}+v\frac{\partial H_1}{\partial y}=H_1\frac{\partial u}{\partial x}+H_2\frac{\partial u}{\partial y}+\mu_0\frac{\partial^2 H_1}{\partial y^2}. \tag{3.40}$$

$$u\frac{\partial N}{\partial x}+v\frac{\partial N}{\partial y}+M_0H_0\tau HN=\frac{\gamma^*}{\rho_j}\frac{\partial^2 N}{\partial y^2}-\frac{k}{\rho_j c}\left(2N+\frac{\partial u}{\partial y}\right). \tag{3.41}$$

Subjected to the boundary conditions:

$$\left.\begin{aligned} &N=-N_0\frac{\partial u}{\partial y},\quad u=cx,\quad v=0,\quad H_2=\frac{\partial H_1}{\partial y}=0,\quad \text{at } y=0,\\ &u=ax,\quad H_1=H_e(x)=H_0x,\quad N\to 0\quad \text{as } y\to\infty. \end{aligned}\right\} \tag{3.42}$$

3.4 Non-dimensionalization

This section consists of non-dimensionalization of the governing equations in the mathematical model.The mathematical model will be transformed into a system of ODEs using the following similarity transformation:

$$\left.\begin{aligned} &v=-\sqrt{\nu c}\,f(\eta), \qquad u=cxf'(\eta), \qquad \eta=\sqrt{\frac{c}{\nu}}\,y,\\ &N=cx\sqrt{\frac{c}{\nu}}\,g(\eta), \qquad H_1=H_0xh'(\eta), \qquad H_2=-H_0\sqrt{\frac{\nu}{c}}\,h(\eta). \end{aligned}\right\} \tag{3.43}$$

Here the dimensionless parameters are defined as:

$$K=\frac{k}{\mu}, \qquad \frac{R_m}{R_e}=\frac{\sigma H_0^2\nu}{\rho c^2}, \qquad R_m=\sigma\mu_0\nu_0 L, \qquad R_e=\frac{\nu_0 L}{\nu}, \qquad d=\frac{H_0^2}{c^2 l}, \qquad \lambda=\frac{\mu_0}{\nu}. \tag{3.44}$$

$$\left(1+\frac{k}{2}\right)=\frac{\gamma^*}{\rho_j}, \qquad \frac{\omega}{\alpha}=\frac{\tau M_0\mu_0\bar{H}}{c}, \qquad \omega=\frac{\tau M_0 H_0^2}{\rho\bar{H}c}, \qquad \beta^*=\frac{k}{\rho j_c}. \tag{3.45}$$

3.4.1 Non-dimesionlization of Continuity Equation

Following derivatives are required to satisfy the continuity equation (3.37):

$$\begin{aligned} \frac{\partial u}{\partial x}&=\frac{\partial}{\partial x}\left(cxf'(\eta)\right)\\ &=cf'(\eta)\cdot\frac{\partial x}{\partial x}\\ &=cf'(\eta). \end{aligned} \tag{3.46}$$

And

$$\begin{aligned}\frac{\partial v}{\partial y} &= \frac{\partial}{\partial y}\left(-\sqrt{c\nu}f(\eta)\right)\\ &= -\sqrt{c\nu}f'(\eta)\cdot\frac{\partial \eta}{\partial y}\\ &= -\sqrt{c\nu}f'(\eta)\cdot\sqrt{\frac{c}{\nu}}\\ &= -cf'(\eta).\end{aligned} \tag{3.47}$$

Using (3.46) and (3.47) in (3.37), we obtain

$$cf'(\eta) - cf'(\eta) = 0. \tag{3.48}$$

The following derivatives are required to satisfy the magnetic flux equation (3.38):

$$\begin{aligned}\frac{\partial H_1}{\partial x} &= \frac{\partial}{\partial x}\left(H_0 x\, h'(\eta)\right)\\ &= H_0 h'(\eta)\cdot\frac{\partial x}{\partial x}\\ &= H_0 h'(\eta).\end{aligned} \tag{3.49}$$

$$\begin{aligned}\frac{\partial H_2}{\partial y} &= \frac{\partial}{\partial y}\left(-H_0\sqrt{\frac{\nu}{c}}\,h(\eta)\right)\\ &= -H_0\sqrt{\frac{\nu}{c}}\,h'(\eta)\cdot\frac{\partial \eta}{\partial y}\\ &= -H_0\sqrt{\frac{\nu}{c}}\,h'(\eta)\cdot\sqrt{\frac{c}{\nu}}\\ &= -H_0 h'(\eta).\end{aligned} \tag{3.50}$$

Using (3.49) and (3.50) in (3.38), we obtain

$$H_0 h'(\eta) - H_0 h'(\eta) = 0. \tag{3.51}$$

3.4.2 Momentum Equation

The momentum equation is expressed as

$$u\frac{\partial u}{\partial x}+v\frac{\partial u}{\partial y}=(\mu+k)\,\frac{1}{\rho}\frac{\partial^2 u}{\partial y^2}-\frac{\sigma}{\rho}\mu_0 H_2^2 u+\frac{k}{\rho}\frac{\partial N}{\partial y} + \frac{1}{\rho M_0 \bar{H}}\left(H_1+\tau N H_2\right)\frac{\partial H_1}{\partial x}+\left(H_2-\tau N H_1\right)\frac{\partial H_2}{\partial x}. \tag{3.52}$$

Derivatives required on the L.H.S of (3.52):

$$\frac{\partial u}{\partial x}=cf', \qquad \frac{\partial u}{\partial y}=cxf''\sqrt{\frac{c}{\nu}}f.$$

Using the above derivatives on the L.H.S of (3.52) gives:

$$\begin{aligned} u\frac{\partial u}{\partial x}+v\frac{\partial u}{\partial y} &= cxf'(cf')-\sqrt{\nu c}\cdot cxf''\sqrt{\frac{c}{\nu}}f \\ &= c^2xf'^2-c^2xf''f. \end{aligned} \tag{3.53}$$

Derivatives required on the R.H.S of (3.52):

$$\frac{\partial^2 u}{\partial y^2}=cxf'''\left(\frac{c}{\nu}\right), \qquad \frac{\partial N}{\partial y}=cx\left(\frac{c}{\nu}\right)g', \qquad \frac{\partial H_1}{\partial x}=H_0h'.$$

Using these derivatives on the R.H.S of (3.52):

$$\left(\frac{\mu+k}{\rho}\right)\frac{c^2x}{\nu}f'''-\left(\frac{\nu\sigma}{\rho}\right)\mu_0H_0^2xh^2f'+\left(\frac{k}{\rho\nu}\right)c^2xg'+\frac{M_0H_0^2xh'^2}{\rho\bar{H}} - \frac{\tau M_0H_0^2cxg}{\rho\bar{H}}hh'. \tag{3.54}$$

Comparing (3.53) with (3.54) leads to:

$$(1+K)f'''=\frac{R_m}{R_e}h^2f'-Kg'-\alpha h'^2+\omega ghh'+f'^2-ff''. \tag{3.55}$$

3.4.3 Megnatic Equation

$$u\frac{\partial H_1}{\partial x}+v\frac{\partial H_1}{\partial y}=H_1\frac{\partial u}{\partial x}+H_2\frac{\partial u}{\partial y}+\mu_0\frac{\partial^2 H_1}{\partial y^2}. \tag{3.56}$$

where,

$$\frac{\partial u}{\partial x}=cf'. \tag{3.57}$$

$$\frac{\partial H_1}{\partial x}=H_0h'. \tag{3.58}$$

$$\frac{\partial u}{\partial y}=cxf''\sqrt{\frac{c}{v}}. \tag{3.59}$$

$$\frac{\partial H_1}{\partial y}=H_0xh''\sqrt{\frac{c}{\nu}}. \tag{3.60}$$

Using (3.57))-(3.60) in (3.56) leads to:

$$cxf'(H_0h')-\sqrt{\nu c}f\left(H_0xh''\sqrt{\frac{c}{v}}\right)=H_0xh'(cf')$$
$$-\left(H_0\sqrt{\frac{\nu}{c}}h\right)\left(cxf''\sqrt{\frac{c}{v}}\right)+\mu_0H_0xh''\sqrt{\frac{c}{v}}.$$

$$\lambda h'''-hf''+h''f=0. \tag{3.61}$$

3.4.4 Microrotation Equation

$$u\frac{\partial N}{\partial x}+v\frac{\partial N}{\partial y}=\frac{\gamma^*}{\rho_j}\frac{\partial^2 N}{\partial y^2}-\frac{k}{\rho_j c}\left(2N+\frac{\partial u}{\partial y}\right)-M_0H_0\tau\bar{H}N. \tag{3.62}$$

$$\eta=\sqrt{\frac{c}{\nu}}y,\quad u=cxf',\quad v=-\sqrt{\nu c}f,\quad N=cx\sqrt{\frac{c}{\nu}}g.$$

Derivatives required to satisfy (3.62):

$$\frac{\partial \eta}{\partial y}=\sqrt{\frac{c}{\nu}}$$

$$\frac{\partial u}{\partial y}=cxf''\sqrt{\frac{c}{\nu}}.$$

$$\frac{\partial N}{\partial x}=c\sqrt{\frac{c}{\nu}}g.$$

$$\frac{\partial N}{\partial y}=\frac{c^2xg'}{\nu}.$$

$$\frac{\partial^2 N}{\partial y^2} = \frac{c^x}{\nu} g'' \sqrt{\frac{c}{\nu}}.[-10pt]$$

Using derivatives on L.H.S of (3.62) implies

$$c^2 x f' g \sqrt{\frac{c}{\nu}} - \sqrt{\nu c} \left(\frac{c^2 x}{\nu} \right) f g',$$

$$= c^2 x f' g \sqrt{\frac{c}{\nu}} - c^2 x f g' \sqrt{\frac{c}{\nu}}. \tag{3.63}$$

Using derivatives on R.H.S of (3.62)

$$\frac{\gamma^*}{\rho_j} \left(\frac{c^2 x}{\nu} g'' \sqrt{\frac{c}{\nu}} \right) - \frac{k}{\rho_j c} \left(2cx \sqrt{\frac{c}{\nu}} g + cx f'' \sqrt{\frac{c}{\nu}} \right) - M_0 H_0 \tau \bar{H} \left(cx \sqrt{\frac{c}{\nu}} \right) g. \tag{3.64}$$

Comparing (3.63) & (3.64), we get

$$\left(1 + \frac{K}{2} \right) g'' = \beta^* \left(2g + f'' \right) - \frac{\omega}{\alpha} g + f' g - f g'. \tag{3.65}$$

3.4.5 Dimensionless Boundary Conditions

The boundary conditions given in (3.42) are converted into their non-dimensional form using the following approach:

(i) $u = cx,$ at $y = 0.$

$\Rightarrow cx f'(\eta) = cx,$

$\Rightarrow f'(\eta) = 1,$ at $\eta = 0.$

(ii) $v = 0,$

$$\Rightarrow \sqrt{\nu c} f(\eta) = 0,$$

$$\Rightarrow f(\eta) = 0, \qquad \text{at } \eta = 0.$$

$$\left.\frac{\partial H_1}{\partial y}\right|_{y=0} = H_2 = 0,$$

$$\Rightarrow H_0 x \left(\sqrt{\frac{c}{\nu}}\right) h''(\eta) = -H_0 \sqrt{\frac{\nu}{c}} h(\eta),$$

$$\Rightarrow H_0 x \left(\sqrt{\frac{c}{\nu}}\right) h''(\eta) = H_0 x,$$

$$\Rightarrow h''(\eta) = h(\eta), \qquad \text{at } \eta = 0.$$

(iii) $N = -N_0 \dfrac{\partial u}{\partial y},$

$$\Rightarrow cx \left(\sqrt{\frac{c}{\nu}}\right) g(\eta) = -N_0 \left(cx f''(\eta) \sqrt{\frac{c}{\nu}}\right),$$

$$\Rightarrow g(\eta) = -\left(\frac{cx\sqrt{\frac{c}{\nu}}}{cx\sqrt{\frac{c}{\nu}}}\right) N_0 f''(\eta),$$

$$\Rightarrow g(\eta) = -N_0 f''(\eta), \qquad \text{at } \eta = 0.$$

(iv) $u = ax,$

$$\Rightarrow cx f'(\eta) = ax,$$

$$\Rightarrow f'(\eta) = \frac{a}{c}, \qquad \text{as } \eta \to \infty.$$

$$H_1 = H_0 x, \qquad \text{as } y \to \infty.$$

$$\Rightarrow H_0 x h'(\eta) = H_0 x, \qquad \text{as } \eta \to \infty.$$

$$\Rightarrow h'(\eta) = 1, \qquad \text{as } \eta \to \infty$$

$$N \to 0, \qquad \text{as } \tilde{y} \to \infty.$$

$$\Rightarrow cx\sqrt{\frac{c}{\nu}} g(\eta) \to 0, \qquad \text{as } \eta \to \infty$$

$$\Rightarrow g(\eta) \to 0, \qquad \text{as } \eta \to \infty.$$

3.4.6 Non-dimensionalization of the Skin-Friction

$$C_f = \frac{\tau_w}{\rho u_w^2}$$

where,

$$\tau_w = (\mu + \eta_1)\frac{\partial u}{\partial y} + \eta_1 N. \tag{3.66}$$

Using similarity variables:

$$\frac{\partial u}{\partial y} = cxf''(\eta)\sqrt{\frac{c}{\nu}}, \qquad N = cx\sqrt{\frac{c}{\nu}}g(\eta).$$

Substitute into (3.66):

$$\begin{aligned}\tau_w &= (\mu + \eta_1)cxf''(\eta)\sqrt{\frac{c}{\nu}} + \eta_1 cx\sqrt{\frac{c}{\nu}}g(\eta),\\ &= cx\sqrt{\frac{c}{\nu}}\left[(\mu + \eta_1)f''(\eta) + \eta_1 g(\eta)\right].\end{aligned}$$

Now substitute into the definition of C_f:

$$C_f = \frac{cx\sqrt{\frac{c}{\nu}}\left[(\mu + \eta_1)f''(\eta) + \eta_1 g(\eta)\right]}{\rho u_w^2}.$$

Since $u_w = cx$, simplify:

$$\begin{aligned}C_f &= \frac{u_w\sqrt{\frac{c}{\nu}}\left[(\mu + \eta_1)f''(\eta) + \eta_1 g(\eta)\right]}{\rho u_w^2},\\ &= \frac{\sqrt{\frac{c}{\nu}}\left[(\mu + \eta_1)f''(\eta) + \eta_1 g(\eta)\right]}{\rho u_w}.\end{aligned}$$

Introduce dimensionless parameters:

$$\begin{aligned}K &= \frac{\eta_1}{\mu}, \quad \text{and} \quad \eta_1 = K\mu,\\ C_f &= \frac{\mu\sqrt{\frac{c}{\nu}}\left[(1 + K)f''(\eta) + Kg(\eta)\right]}{\rho u_w}.\end{aligned}$$

Since $\nu = \mu/\rho$:

$$C_f = \frac{\nu\sqrt{\frac{c}{\nu}}\,[(1+K)f''(\eta) + Kg(\eta)]}{u_w},$$
$$= \frac{\sqrt{\nu c}\,[(1+K)f''(\eta) + Kg(\eta)]}{u_w}.$$

Now express c in terms of u_w and x:

$$c = \frac{u_w}{x} \quad \Rightarrow \quad \sqrt{c} = \sqrt{\frac{u_w}{x}}.$$

$$C_f = \frac{\sqrt{\nu \cdot \frac{u_w}{x}}\,[(1+K)f''(\eta) + Kg(\eta)]}{u_w},$$

$$= \frac{\sqrt{\frac{\nu u_w}{x}}\,[(1+K)f''(\eta) + Kg(\eta)]}{u_w},$$

$$= \frac{[(1+K)f''(\eta) + Kg(\eta)]}{\sqrt{\nu}\sqrt{u_w}\sqrt{x}},$$

$$= \frac{[(1+K)f''(\eta) + Kg(\eta)]}{\sqrt{Re_x}}, \quad \text{where } Re_x = \frac{u_w x}{\nu}.$$

$$\Rightarrow \sqrt{Re_x}\,C_f = (1+K)f''(0) + Kg(0).$$

3.5 Method of Solution

In order to solve the ODEs by the shooting method,the following notations have been taken:

$$f(\eta) = Z_1, \quad f'(\eta) = Z_2, \quad f''(\eta) = Z_3, \quad f'''(\eta) = Z_3'(\eta),$$
$$h(\eta) = Z_4, \quad h'(\eta) = Z_5, \quad h''(\eta) = Z_6, \quad h'''(\eta) = Z_6',$$
$$g(\eta) = Z_7, \quad g'(\eta) = Z_8, \quad g''(\eta) = Z_8'.$$

The system of equations (3.55), (3.61) and (3.65) can be represented in the form of the following first-order ODEs:

$$
\begin{aligned}
Z_1' &= Z_2 && Z_1(0) = 0,\\
Z_2' &= Z_3 && Z_2(0) = 1,\\
Z_3' &= \frac{1}{1+K}\left[\left(\frac{R_m}{R_e}\right) Z_4^2 Z_2 - K Z_8 - \alpha Z_5^2 + \omega Z_7 Z_4 Z_5 + \right.\\
&\quad \left. Z_2^2 - Z_1 Z_3 \right] && Z_3(0) = p,\\
Z_4' &= Z_5 && Z_4(0) = 0,\\
Z_5' &= Z_6 && Z_5(0) = q,\\
Z_6' &= \frac{1}{\lambda}\left(Z_4 Z_3 - Z_6 Z_1\right) && Z_6(0) = 0,\\
Z_7' &= Z_8 && Z_7(0) = -N_0 p,\\
Z_8' &= \frac{2}{2+K}\left[\beta^*(2Z_7 + Z_3) - \frac{\omega}{\alpha} Z_7 + Z_2 Z_7 - Z_1 Z_8\right] && Z_8(0) = r.
\end{aligned}
$$

The missing conditions p, q, and r are assumed to satisfy the following relation:

$$
\left.
\begin{aligned}
Z_2(p,q,r) &= \frac{a}{c},\\
Z_5(p,q,r) &= 1,\\
Z_7(p,q,r) &= 0.
\end{aligned}
\right\} \tag{3.67}
$$

To find the solution of the above algebraic equations, Newton's method is employed using the following scheme:

$$
\begin{bmatrix} p^{n+1} \\ q^{n+1} \\ r^{n+1} \end{bmatrix} = \begin{bmatrix} p^{n} \\ q^{n} \\ r^{n} \end{bmatrix} - \begin{bmatrix} \frac{\partial Z_2}{\partial p} & \frac{\partial Z_2}{\partial q} & \frac{\partial Z_2}{\partial r} \\ \frac{\partial Z_5}{\partial p} & \frac{\partial Z_5}{\partial q} & \frac{\partial y_5}{\partial r} \\ \frac{\partial Z_7}{\partial p} & \frac{\partial Z_7}{\partial q} & \frac{\partial Z_7}{\partial r} \end{bmatrix}_n^{-1} \begin{bmatrix} Z_2 \\ Z_5 \\ Z_7 \end{bmatrix}_n . \tag{3.68}
$$

For above formula we introduced the following notations:

$$
\begin{aligned}
&\frac{\partial Z_1}{\partial p} = Z_9, \quad \frac{\partial Z_2}{\partial p} = Z_{10}, \quad \frac{\partial Z_3}{\partial p} = Z_{11},\\
&\frac{\partial Z_4}{\partial p} = Z_{12}, \quad \frac{\partial Z_5}{\partial p} = Z_{13}, \quad \frac{\partial Z_6}{\partial p} = Z_{14},\\
&\frac{\partial Z_7}{\partial p} = Z_{15}, \quad \frac{\partial Z_8}{\partial p} = Z_{16}.
\end{aligned}
$$

$$\frac{\partial Z_1}{\partial q} = Z_{17}, \quad \frac{\partial Z_2}{\partial q} = Z_{18}, \quad \frac{\partial Z_3}{\partial q} = Z_{19},$$

$$\frac{\partial Z_4}{\partial q} = Z_{20}, \quad \frac{\partial Z_5}{\partial q} = Z_{21}, \quad \frac{\partial Z_6}{\partial q} = Z_{22},$$

$$\frac{\partial Z_7}{\partial q} = Z_{23}, \quad \frac{\partial Z_8}{\partial q} = Z_{24}.$$

$$\frac{\partial Z_1}{\partial r} = Z_{25}, \quad \frac{\partial Z_2}{\partial r} = Z_{26}, \quad \frac{\partial Z_3}{\partial r} = Z_{27},$$

$$\frac{\partial Z_4}{\partial r} = Z_{28}, \quad \frac{\partial Z_5}{\partial r} = Z_{29}, \quad \frac{\partial Z_6}{\partial r} = Z_{30},$$

$$\frac{\partial Z_7}{\partial r} = Z_{31}, \quad \frac{\partial Z_8}{\partial r} = Z_{32}.$$

With the revised notation and the updated expressions for the partial derivatives, Newton's iterative scheme takes the following form:

$$\begin{bmatrix} p^{n+1} \\ q^{n+1} \\ r^{n+1} \end{bmatrix} = \begin{bmatrix} p^n \\ q^n \\ r^n \end{bmatrix} - \begin{bmatrix} Z_{10} & Z_{18} & Z_{26} \\ Z_{13} & Z_{21} & Z_{29} \\ Z_{15} & Z_{23} & Z_{31} \end{bmatrix}^{-1} \begin{bmatrix} Z_2 \\ Z_5 \\ Z_7 \end{bmatrix}. \tag{3.69}$$

The convergence criterion for Newton's method is defined as follows:

$$\max\{|Z_2(\eta_\infty)|, |Z_5(\eta_\infty)|, |Z_7(\eta_\infty)|\} < \epsilon, \tag{3.70}$$

where $\epsilon > 0$ is an arbitrarily small positive number. From now onwards, ϵ is taken as 10^{-10}.

3.5.1 Numerical Results

This section presents the physical behavior of various profiles, including the hydrodynamic velocity profile, magnetic induction and micro-rotational velocity profile, by considering variations in key physical parameters such as the magnetic Reynolds number (Rm), the micro-polar parameter (K), and the micro-polar coupling parameter.

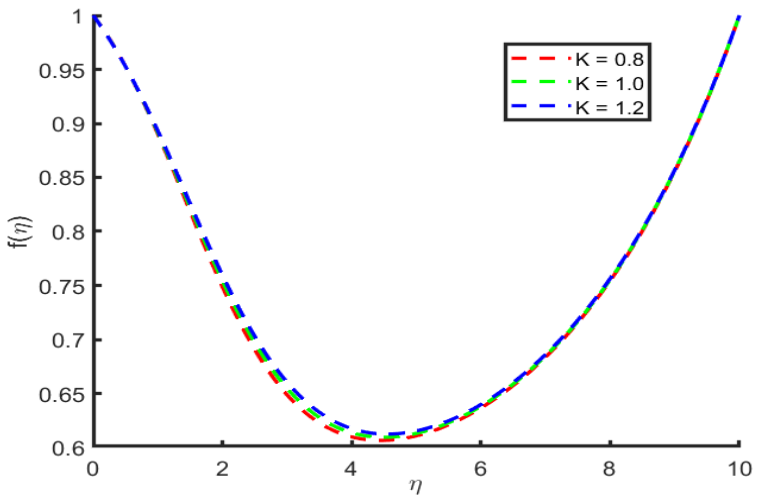

FIGURE 3.2: Velocity profile for varying micro-polar coupling parameter.

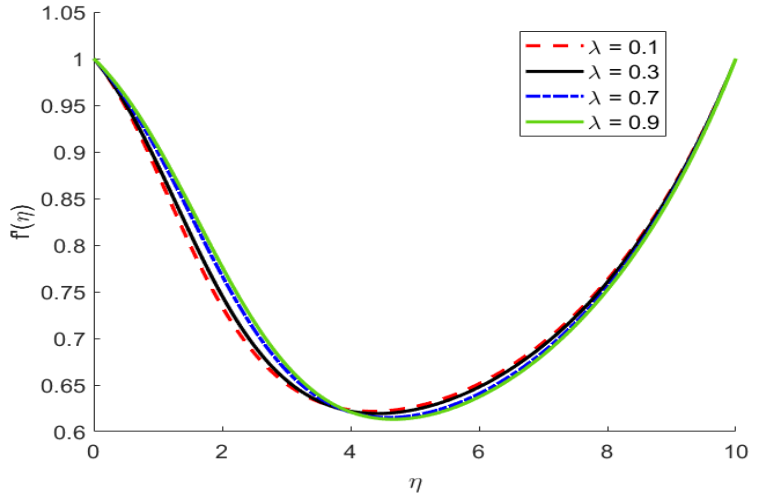

FIGURE 3.3: Velocity profile for varying magnetization parameter.

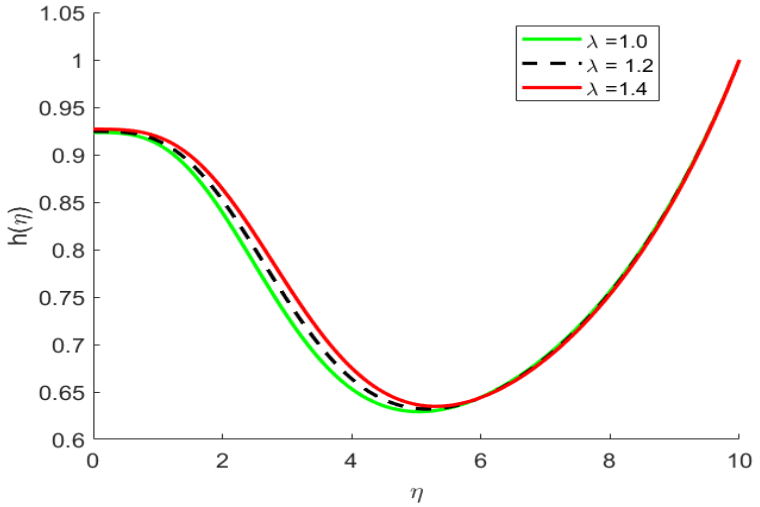

FIGURE 3.4: Magnetic induction profile for varying magnetization parameter.

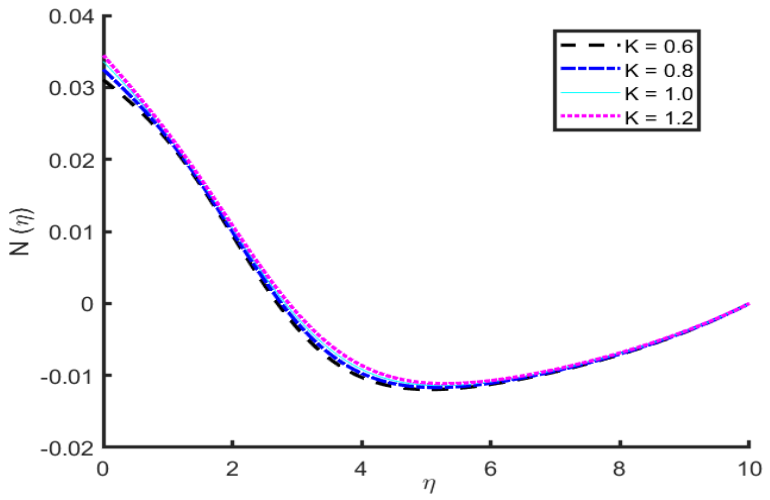

FIGURE 3.5: Micro-rotation profile for varying micro-polar coupling parameter.

3.5.2 Hydrodynamic Velocity Profile

As shown in Figure 3.2, A clear effect of increasing the micropolar parameter K is observed in the elevation of the velocity profile. As the micropolar parameter increases, the minimum value of the velocity curve becomes higher, and the entire profile shifts slightly upward. This behavior can be attributed to the fact that the micropolar parameter represents the coupling between the microrotation of microelements and the linear motion of the fluid.

As a result, the effective resistance to flow is reduced, allowing the fluid to experience a slight boost in velocity throughout the boundary layer. In physical terms, micropolar effects assist the fluid in flowing more easily, leading to a higher velocity compared to a fluid with a lower or zero micropolar parameter.

This confirms that the microrotation characteristics of the fluid play a significant role in improving the overall flow behavior within the boundary layer.

Figure 3.3 shows the Effect of the Magnetization Parameter λ on the Hydrodynamic Velocity Profile $f'(\eta)$: The graph presents the variation of the hydrodynamic velocity $f'(\eta)$. The influence of the magnetization parameter λ on the velocity profile is evident. As λ increases, the minimum value of $f'(\eta)$ becomes lower, and the velocity profile shifts downward. In other words, higher values of λ suppress the hydrodynamic velocity across the boundary layer. Physically, the magnetization

parameter λ characterizes the interaction between the magnetic field and the flow. As λ increases, the magnetic forces exert a stronger resistive effect (often called the Lorentz force) against the fluid motion, thereby reducing the overall velocity. This magnetic damping effect becomes more prominent at higher λ values, indicating that stronger magnetization slows down the fluid flow. In conclusion, increasing the magnetization parameter λ leads to a suppression of the hydrodynamic velocity profile $f'(\eta)$. This highlights the significant role of magnetic effects in controlling and stabilizing the flow behavior within the boundary layer.

3.5.3 Magnetic Induction Profile

As the magnetization parameter λ increases, the magnetic induction h shows a slight increase across the domain (see Figure 3.4). The curves generally follow a similar pattern, initially decreasing, reaching a minimum, and then increasing again. Higher values of λ (e.g., $\lambda = 1.4$) result in a greater magnitude of h, particularly in the rising phase beyond the minimum point. The influence of λ becomes more pronounced in regions where the curvature of h changes. This behavior indicates that stronger magnetization enhances the magnetic induction throughout the domain, affecting the stability and distribution of the magnetic field in the system.

3.5.4 Micro-Rotational Velocity Profile

The Figure 3.5 shows how the microrotational velocity $N(\eta)$ changes with respect to the similarity variable η for different values of the micropolar parameter K.

As η increases (moving away from the surface), the microrotation $N(\eta)$ first decreases, becomes negative, and then gradually increases again. This indicates how the spinning motion of fluid particles evolves through the boundary layer.

An increase in the micropolar parameter K leads to a reduction in microrotation intensity. In other words, the fluid exhibits less rotational motion. Therefore, higher values of K reduce microrotational effects and cause the fluid to behave

more like a Newtonian fluid.

The skin-friction coefficient $f''(0)$ quantifies the shear stress exerted by the fluid at the boundary surface. It reflects how variations in the physical parameters influence the velocity gradient at the wall.

TABLE 3.1: Skin-friction coefficient $f''(0)$ for varying physical parameters.

S No.	ω	β^*	λ	K	$f''(0)$
1	0	0.1	0.5	1	-0.85046062
2	0.1	0.1	0.5	1	-0.825250784
3	0.25	0.1	0.5	1	-0.834020274
4	0.3	0.1	0.5	1	-0.817774763
5	0	0.15	0.5	1	-0.837823138
6	0.1	0.15	0.5	1	-0.808335645
7	0.3	0.15	0.5	1	-0.794175473

An increase in the MMR parameter ω generally leads to a reduction in the magnitude of the skin-friction coefficient. For example, as ω increases from 0 to 0.3 (with other parameters held constant), $f''(0)$ changes from -0.8504 to -0.8177. This reduction indicates that rotational effects introduce centrifugal forces, which redistribute momentum away from the boundary layer, thereby reducing the shear stress at the wall. Increasing β^* from 0.1 to 0.15 results in a decrease in the magnitude of the skin-friction coefficient. This implies that micropolar effects, which account for the micro-rotational behavior of fluid particles, enhance the momentum transport within the fluid and subsequently lower the wall shear stress.

Chapter 4

Magneto-Micropolar Boundary Layer Flow with Chemically Reactive Process

4.1 Introduction

This chapter builds upon the model developed by Khan and Hameed[9], which examined heat transfer within the framework of magnetohydrodynamic (MHD) micropolar flow. In this chapter , we e investigate the influence of micromagnetorotation (MMR) on concentration in a chemically reacting process, specifically within the context of the micropolar boundary layer. The objective of this study is to investigate how key energy and concentration-related parameters affect flow characteristics such as velocity, temperature, concentration profiles, and skin friction. The original nonlinear partial differential equations (PDEs) are first transformed into a set of dimensionless ordinary differential equations (ODEs) using similarity transformations. These equations are subsequently solved using the shooting technique.

At the conclusion of this chapter, the results are thoroughly analyzed and discussed. This analysis is presented through detailed graphical representations,

which emphasize the influence of significant parameters on the velocity, temperature, and concentration profiles within the micropolar flow system. By examining these profiles, we aim to provide a deeper understanding of the underlying physical processes and the role of MMR in the system's behavior.

4.2 Mathematical Model

The vector form of the governing equations is as follow:

$$\nabla \cdot \mathbf{U} = 0, \tag{4.1}$$

$$\nabla \cdot \mathbf{H} = 0, \tag{4.2}$$

$$\begin{aligned} \rho\frac{d\mathbf{U}}{dt} + \mathbf{U}\cdot\nabla\mathbf{U} + \nabla p = \eta\nabla^2\mathbf{U} + 2\eta_1\nabla\times(\mathbf{W}-\mathbf{w}) \\ + (\nabla\times\mathbf{H})\times\mathbf{B} + (\mathbf{M}\cdot\nabla)\mathbf{H} + \mathbf{M}\times(\nabla\times\mathbf{H}), \end{aligned} \tag{4.3}$$

$$\rho\frac{d\mathbf{H}}{dt} + \mathbf{U}\cdot\nabla\mathbf{H} = \eta\nabla^2\mathbf{H} + \mathbf{H}\cdot\nabla\mathbf{U}, \tag{4.4}$$

$$l\frac{d\mathbf{W}}{dt} = \gamma\nabla^2\mathbf{W} + 4\eta_1(\mathbf{w}-\mathbf{W}) + \mathbf{M}\times\mathbf{H} - \mathbf{U}\cdot\nabla\mathbf{W}, \tag{4.5}$$

$$\frac{Q}{\rho c_p}(\mathbf{T}-\mathbf{T}_\infty) + \frac{1}{\rho c_p}\nabla\cdot(0,q_r) = u\cdot\nabla\mathbf{T} - \kappa\boldsymbol{\Delta}\mathbf{T}, \tag{4.6}$$

$$\mathbf{D}\,\boldsymbol{\Delta}C = u\cdot\boldsymbol{\nabla}C, \tag{4.7}$$

$$\mathbf{B} - \mathbf{M} = \mu_0\mathbf{H}, \tag{4.8}$$

$$\mathbf{M}\cdot\frac{\bar{H}}{\mathbf{H}} = M_0(\mathbf{I} - \tau\mathbf{W}\cdot\boldsymbol{\epsilon}), \tag{4.9}$$

and

$$\mathbf{J} = \sigma\left(\mathbf{E} + \mathbf{U}\times\mathbf{B}\right). \tag{4.10}$$

D, κ, Q, and q_r are molecular diffusivity, thermal diffusivity, dimensional heat source, and radiative heat flux, respectively.

4.3 Governing Equations in the Operator-Form

The derivations of the continuity equations, momentum equation, magnetic induction equation, and micro-rotation equation in operator form have already been discussed in Chapter 3. In this section, we present the process of transforming the energy and concentration equations from vector form into component form.

4.3.1 Energy Equation

$$\begin{aligned}
\frac{Q}{\rho c_p}(T-T_\infty)+\frac{1}{\rho c_p}\nabla\cdot(0,q_r) &= u\nabla T-\kappa\Delta T,\\
&= \frac{Q}{\rho c_p}(T-T_\infty)+\frac{1}{\rho c_p}\left(\frac{\partial}{\partial x},\frac{\partial}{\partial y}\right)(0,q_r)\\
&= (u,v)\left(\frac{\partial T}{\partial x},\frac{\partial T}{\partial y}\right)-\kappa\left(\frac{\partial^2 T}{\partial x^2}+\frac{\partial^2 T}{\partial y^2}\right)\\
= \frac{Q}{\rho c_p}(T-T_\infty)+\frac{1}{\rho c_p}\left(0,\frac{\partial q_r}{\partial y}\right) &= u\frac{\partial T}{\partial x}+v\frac{\partial T}{\partial y}-\kappa\frac{\partial^2 T}{\partial y^2}\\
= \frac{Q}{\rho c_p}(T-T_\infty)+\frac{1}{\rho c_p}\frac{\partial q_r}{\partial y} &= \left(u\frac{\partial T}{\partial x}+v\frac{\partial T}{\partial y}\right)-\kappa\frac{\partial^2 T}{\partial y^2}. \qquad (4.11)
\end{aligned}$$

4.3.2 Concentration Equation

$$\begin{aligned}
D\Delta C &= u\cdot\nabla C,\\
D\left(\frac{\partial^2 C}{\partial x^2}+\frac{\partial^2 C}{\partial y^2}\right) &= (u,v)\cdot\left(\frac{\partial C}{\partial x},\frac{\partial C}{\partial y}\right),\\
D\left(\frac{\partial^2 C}{\partial y^2}\right) &= u\frac{\partial C}{\partial x}+v\frac{\partial C}{\partial y},\\
D\frac{\partial^2 C}{\partial y^2} &= u\frac{\partial C}{\partial x}+v\frac{\partial C}{\partial y}. \qquad (4.12)
\end{aligned}$$

The continuity, momentum, magnetic induction, micro-rotation, energy, and concentration equations governing the aforementioned problem under the usual boundary layer approximations are as follows :

Continuity Equation:

$$\frac{\partial u}{\partial x}+\frac{\partial v}{\partial y}=0. \qquad (4.13)$$

$$\frac{\partial H_1}{\partial x} + \frac{\partial H_2}{\partial y} = 0. \tag{4.14}$$

Momentum Equation:

$$\begin{aligned} v\frac{\partial u}{\partial x} + v\frac{\partial u}{\partial y} = (\mu + k)\,\frac{1}{\rho}\frac{\partial^2 u}{\partial y^2} - \frac{\sigma}{\rho}\mu_0 H_2^2 u + \frac{k}{\rho}\frac{\partial N}{\partial y} \\ + \frac{1}{\rho M_0 \bar{H}}\left(H_1 + \tau N H_2\right)\frac{\partial H_1}{\partial x} + \left(H_2 - \tau N H_1\right)\frac{\partial H_2}{\partial x}. \end{aligned} \tag{4.15}$$

Magnetic Induction Equation:

$$\nu\frac{\partial H_1}{\partial x} + v\frac{\partial H_1}{\partial y} = H_1\frac{\partial u}{\partial x} + H_2\frac{\partial u}{\partial y} + \mu_0\frac{\partial^2 H_1}{\partial y^2}. \tag{4.16}$$

Microrotation Equation:

$$M_0 H_0 \tau H N + \frac{k}{\rho_j}\left(2N + \frac{\partial u}{\partial y}\right) = \nu\frac{\partial N}{\partial x} + v\frac{\partial N}{\partial y} - \frac{\gamma^*}{\rho_j}\frac{\partial^2 N}{\partial y^2}. \tag{4.17}$$

Energy Equation:

$$\frac{Q}{\rho c_p}(T - T_\infty) + \frac{1}{\rho c_p}\frac{\partial q_r}{\partial y} = u\frac{\partial T}{\partial x} + V\frac{\partial T}{\partial y} - \kappa\frac{\partial^2 T}{\partial y^2}. \tag{4.18}$$

Concentration Equation:

$$D\frac{\partial^2 C}{\partial y^2} = u\frac{\partial C}{\partial x} + v\frac{\partial C}{\partial y}. \tag{4.19}$$

Boundary Conditions: The system is subjected to the following boundary conditions:

$$\left.\begin{array}{lll} u = cx, \quad v = 0, \quad N = -N_0\dfrac{\partial u}{\partial y}, \quad \dfrac{\partial H_1}{\partial y} = 0, \quad H_2 = 0, & & \\ T = T_w, \quad C = C_w, & & \text{at } y = 0, \\ u \to ax, \quad H_1 \to H_0 x, \quad N \to 0, \quad T \to T_\infty, \quad C \to C_\infty, & & \text{as } y \to \infty. \end{array}\right\} \tag{4.20}$$

4.4 Non-Dimensionalization

The mathematical model will be transformed into a system of ordinary differential equations (ODEs) using the following similarity transformation:

$$\left.\begin{aligned} v = -\sqrt{\nu c} f(\eta), \quad u = x f'(\eta) c, \qquad\qquad \eta = \sqrt{\frac{c}{\nu}} y, \\ N = cx\sqrt{\frac{c}{\nu}} g(\eta), \quad H_1 = H_0 x h'(\eta), \quad H_2 \ = -h(\eta) \cdot H_0 \sqrt{\frac{\nu}{c}}. \end{aligned}\right\} \tag{4.21}$$

$$T = T_\infty - (T_w - T_\infty)\theta(\eta), \quad T^4 = 4T_\infty^3 T - 3T_\infty^4, \quad C = C_\infty + C_0 x \phi(\eta). \tag{4.22}$$

The symbol η represents the similarity variable.The velocity components in the x and y directions are denoted by u and v, respectively.While θ and ϕ represents dimensionless temprature and concentration respectively, N represents micro-rotation.

Non-dimesionlization of equations (4.13)-(4.17) has already been discussed in Chapter 3.

4.4.1 Energy Equation

$$u\frac{\partial T}{\partial x} + v\frac{\partial T}{\partial y} = \kappa\frac{\partial^2 T}{\partial y^2} - \frac{1}{\rho c_p}\frac{\partial q_r}{\partial y} + \frac{Q}{\rho c_p}(T - T_\infty),$$

We introduce the similarity transformations:

$$T = T_\infty + (T_w - T_\infty)\,\theta(\eta),$$

$$\eta = \sqrt{\frac{c}{\nu}}\, y,$$

where $\theta(\eta)$ is the dimensionless temperature function.

The radiative heat flux is given by

$$q_r = \frac{4\sigma}{3k^*}\frac{\partial T^4}{\partial y},$$

where σ is the Stefan–Boltzmann constant and k^* is the mean absorption coefficient.

Assuming the temperature differences within the flow are small, we linearize T^4 using a Taylor series about T_∞:

$$T^4 \approx T_\infty^4 + 4T_\infty^3(T - T_\infty)$$

Thus,

$$\frac{\partial T^4}{\partial y} \approx 4T_\infty^3 \frac{\partial T}{\partial y}.$$

Substituting back in relation for radiative heat flux,

$$q_r = \frac{16\sigma T_\infty^3}{3k^*} \frac{\partial T}{\partial y}.$$

Now, differentiating radiative heat flux with respect to y:

$$\frac{\partial q_r}{\partial y} = \frac{16\sigma T_\infty^3}{3k^*} \frac{\partial^2 T}{\partial y^2}.$$

Derivatives required to satisfy energy equation

$$u = cxf'(\eta), \quad v = -\sqrt{\nu c}\, f(\eta),$$

$$\frac{\partial T}{\partial x} = (T_w - T_\infty)\frac{\partial \theta}{\partial x} = 0 \quad (\text{since } \theta = \theta(\eta)),$$

$$\frac{\partial T}{\partial y} = (T_w - T_\infty)\frac{d\theta}{d\eta}$$

$$\frac{\partial^2 T}{\partial y^2} = (T_w - T_\infty)\frac{c}{\nu}\theta''.$$

Substituting all into the energy equation:

Left-hand side implies

$$u\frac{\partial T}{\partial x} + v\frac{\partial T}{\partial y} = cxf'(0) + \left(-\sqrt{\nu c}f\right)\left((T_w - T_\infty)\sqrt{\frac{c}{\nu}}\,\theta'\right),$$

$$= -c(T_w - T_\infty)f\theta'. \tag{4.23}$$

Right-hand side implies

$$\kappa\frac{\partial^2 T}{\partial y^2} - \frac{1}{\rho c_p}\frac{\partial q_r}{\partial y} + \frac{Q}{\rho c_p}(T - T_\infty),$$

$$= \left(\kappa + \frac{16\sigma T_\infty^3}{3k^*\rho c_p}\right)(T_w - T_\infty)\frac{c}{\nu}\,\theta'' + \frac{Q}{\rho c_p}(T_w - T_\infty)\theta. \tag{4.24}$$

Comparing (4.23) and (4.24) we get

$$-cf\theta' = \left(\kappa + \frac{16\sigma T_\infty^3}{3k^*\rho c_p}\right)\frac{c}{\nu}\,\theta'' + \frac{Q}{\rho c_p}\theta. \tag{4.25}$$

Dividing throughout (4.25) by c and multiplying by ν, we get

$$-f\theta' = \left(\frac{\kappa}{\nu} + \frac{16\sigma T_\infty^3}{3k^*\nu\rho c_p}\right)\theta'' + \frac{Q\nu}{c\rho c_p}\theta.$$

The dimensionless parameters are

$$\mathrm{Pr} = \frac{\nu}{\kappa}, \quad \text{(Prandtl number)}$$

$$R = \frac{4\sigma T_\infty^3}{k^*\kappa\rho c_p}, \quad \text{(Radiation parameter)}$$

$$S = \frac{Q\nu}{c\rho c_p}. \quad \text{(Heat source parameter)}$$

Thus, the energy equation becomes:

$$-\mathrm{Pr}\, f\theta' = \left(1 + \frac{4}{3}R\right)\theta'' + S\theta,$$

or equivalently,

$$\frac{\left(1 + \frac{4}{3}R\right)}{\mathrm{Pr}}\theta'' + f\theta' + S\theta = 0. \tag{4.26}$$

4.4.2 Concentration Equation

$$u\frac{\partial C}{\partial x} + v\frac{\partial C}{\partial y} = D\frac{\partial^2 C}{\partial y^2}, \tag{4.27}$$

We introduce the following similarity transformations:

$$u = cxf'(\eta), \quad v = -\sqrt{\nu c}\, f(\eta), \quad \eta = \sqrt{\frac{c}{\nu}}\, y, \quad C = C_\infty + C_0 x\, \phi(\eta).$$

From these transformations, the partial derivatives become

$$\frac{\partial C}{\partial x} = C_0 \phi(\eta),$$

$$\frac{\partial C}{\partial y} = C_0 x \phi'(\eta) \sqrt{\frac{c}{\nu}},$$

$$\frac{\partial^2 C}{\partial y^2} = C_0 x \phi''(\eta) \frac{c}{\nu}.$$

Substituting these into the left-hand side of the concentration equation implies

$$u\frac{\partial C}{\partial x} + v\frac{\partial C}{\partial y} = (cxf')\,(C_0\phi) + \left(-\sqrt{\nu c}\, f\right)\left(C_0 x \phi' \sqrt{\frac{c}{\nu}}\right),$$

simplifying,

$$= C_0 cx f'\phi - C_0 cx f \phi'.$$

Substituting into the right-hand side of the concentration equation implies

$$D\frac{\partial^2 C}{\partial y^2} = D\left(C_0 x \phi'' \frac{c}{\nu}\right) = C_0 x D \frac{c}{\nu}\phi''.$$

Thus, the governing equation becomes

$$C_0 cx(f'\phi - f\phi') = C_0 x D \frac{c}{\nu}\phi'',$$

Dividing both sides by $C_0 cx$ (assuming $C_0 \neq 0$, $c \neq 0$, $x \neq 0$) gives

$$f'\phi - f\phi' = \frac{D}{\nu}\phi'',$$

Introducing the Schmidt number

$$S_c = \frac{\nu}{D},$$

we have

$$\phi'' = S_c(f'\phi - f\phi'),$$

Thus, the non-dimensional concentration equation is

$$\phi'' = S_c(f'\phi - f\phi'). \tag{4.28}$$

4.4.3 Non-dimensionalization of Boundary Conditions

The boundary conditions for equations (4.15)-(4.17) have already been nondimensionalized in Chapter 3.Here we will nondimensionalized the corresponding boundary conditions for equations (4.18) and (4.19). The boundary conditions for energy equation are non-dimensionalized as follows :

$$\begin{aligned}
& T = T_w, && \text{at} \quad y = 0. \\
\Rightarrow \quad & (T_w - T_\infty)\theta(\eta) + T_\infty = T_w, && \text{at} \quad \eta = 0. \\
\Rightarrow \quad & (T_w - T_\infty)\theta(\eta) = T_w - T_\infty, && \text{at} \quad \eta = 0. \\
\Rightarrow \quad & \theta(\eta) = 1, && \text{at} \quad \eta = 0. \\
& T = T_\infty, && \text{as} \quad y \to \infty. \\
\Rightarrow \quad & (T_w - T_\infty)\theta(\eta) + T_\infty \to T_\infty, && \text{as} \quad \eta \to \infty. \\
\Rightarrow \quad & \theta(\eta) \to 0, && \text{as} \quad \eta \to \infty.
\end{aligned}$$

The boundary conditions for the concentration equation are non-dimensionalized as follows:

$$\begin{aligned}
& C = C_w, && \text{at} \quad y = 0. \\
\Rightarrow \quad & C_\infty + (C_w - C_\infty)\,\phi(\eta) = C_w, && \text{at} \quad \eta = 0. \\
\Rightarrow \quad & \phi(\eta) = 1, && \text{at} \quad \eta = 0.
\end{aligned}$$

$$C \to C_\infty, \qquad \text{as} \quad y \to \infty.$$

$$\Rightarrow \quad C_\infty + (C_w - C_\infty)\,\phi(\eta) \to C_\infty, \qquad \text{as} \quad \eta \to \infty.$$

$$\Rightarrow \quad \phi(\eta) \to 0, \qquad \text{as} \quad \eta \to \infty.$$

4.4.4 Non-Dimensionalization of the Sherwood Number

The local Sherwood number, representing the non-dimensional mass transfer rate at the surface, is defined as

$$Sh_x = \frac{x j_s}{D(C_w - C_\infty)}$$

$$= -\frac{x}{(C_w - C_\infty)} \left(\frac{\partial C}{\partial y}\right)_{y=0}$$

$$= -\frac{x}{(C_w - C_\infty)} \left[(C_w - C_\infty)\sqrt{\frac{u_w}{\nu x}} \left(\frac{d\phi}{d\eta}\right)_{\eta=0}\right]$$

$$= -x\sqrt{\frac{u_w}{\nu x}} \left(\frac{d\phi}{d\eta}\right)_{\eta=0}$$

$$= -\sqrt{\frac{u_w x}{\nu}} \left(\frac{d\phi}{d\eta}\right)_{\eta=0}$$

$$= -\sqrt{Re_x} \left(\frac{d\phi}{d\eta}\right)_{\eta=0}$$

4.4.5 Non-dimensionalization of the Nusselt Number

The local Nusselt number is defined by

$$\begin{aligned} Nu_x &= \frac{q_w x}{k(T_w - T_\infty)} \\ &= -\left(\frac{x}{T_w - T_\infty}\right)\left(\frac{\partial T}{\partial y}\right)_{y=0} \\ &= -\left(\frac{x}{T_w - T_\infty}\right)\left[(T_w - T_\infty)\sqrt{\frac{u_w}{\nu x}}\left(\frac{d\theta}{d\eta}\right)_{\eta=0}\right] \\ &= -x\sqrt{\frac{u_w}{\nu x}}\left(\frac{d\theta}{d\eta}\right)_{\eta=0} \\ &= -\sqrt{\frac{u_w x}{\nu}}\left(\frac{d\theta}{d\eta}\right)_{\eta=0} \\ &= -\sqrt{Re_x}\left(\frac{d\theta}{d\eta}\right)_{\eta=0} \end{aligned}$$

$$(1+K)f''' = f'^2 - ff'' - \alpha h'^2 + \left(\frac{R_m}{R_e}\right)h^2 f' - Kg' + \omega g h h', \tag{4.29}$$

$$\lambda h''' = hf'' - h''f, \tag{4.30}$$

$$\left(1 + \frac{K}{2}\right)g'' = \beta^*\left(2g + f''\right) - f'g - \frac{\omega}{\alpha}g - fg', \tag{4.31}$$

$$\frac{\left(1 + \frac{4}{3}R\right)}{\mathrm{Pr}}\theta'' + f\theta' + S\theta = 0, \tag{4.32}$$

$$\phi'' = S_c(f'\phi - f\phi'). \tag{4.33}$$

4.5 Method of Solution

In order to solve the ODE (4.32) by the shooting method, the following notation has been used:

$$\theta = z_1, \quad \theta' = z_1' = z_2, \quad \theta'' = z_2'. \tag{4.34}$$

The system of equations can be rewritten as the following set of first-order ordinary differential equations (ODEs):

$$\begin{aligned} z_1' &= z_2, \\ z_2' &= -\frac{3}{3+4R} P_r \left(f z_2 + S z_1 \right), \end{aligned} \tag{4.35}$$

with the initial conditions:

$$z_1(0) = 1, \quad z_2(0) = s, \tag{4.36}$$

The initial value problem (IVP) described above will be numerically solved using the fourth-order Runge-Kutta (RK-4) method. The unknown initial condition "s" is estimated based on the following relation:

$$z_1(\eta_\infty)_s = 0. \tag{4.37}$$

The Newton method is employed to solve the system using the following iterative scheme:

$$s_{n+1} = s_n - \frac{z_1(\eta_\infty)_s}{z'(\eta_\infty)_s}. \tag{4.38}$$

The missing condition 's' will be updated using Newton's method, and the process will continue until the criterion $|z_1(\eta_\infty)_s| < \epsilon$ is met.

For the equation (4.33) the following notation will be used

$$\phi = w_1, \phi' \ = w_1' = w_2, \phi'' = w_2'. \tag{4.39}$$

The system of equations can be represented as the following set of first-order ordinary differential equations (ODEs):

$$w_1' = w_2,$$

$$w_2' = S_c \left(f' w_1 - f w_2 \right). \tag{4.40}$$

With the initial conditions:

$$w_1(0) = 1, \quad w_2(0) = t. \tag{4.41}$$

The initial value problem (IVP) outlined above will be numerically solved using the fourth-order Runge-Kutta (RK-4) method.

The missing condition 't' is assumed to satisfy the following relation

$$w_1(\eta_\infty)_t = 0. \tag{4.42}$$

Newton's method, employing the following iterative scheme, is utilized to solve the system:

$$t_{n+1} = t_n - \frac{w_1(\eta_\infty)_t}{w_1'(\eta_\infty)_t}. \tag{4.43}$$

The missing condition 't' will be updated using Newton's method, and the process will continue until the criterion $|w_1(\eta_\infty)_t| < \epsilon$ is met.

4.6 Numerical Results And Discussion

During the transformation of the governing partial differential equations (PDEs) into a system of ordinary differential equations (ODEs), several physical parameters appear.

The effects of these parameters on the hydrodynamic velocity, microrotational velocity, magnetic induction, temperature distribution, and concentration profile are carefully studied using graphical results.

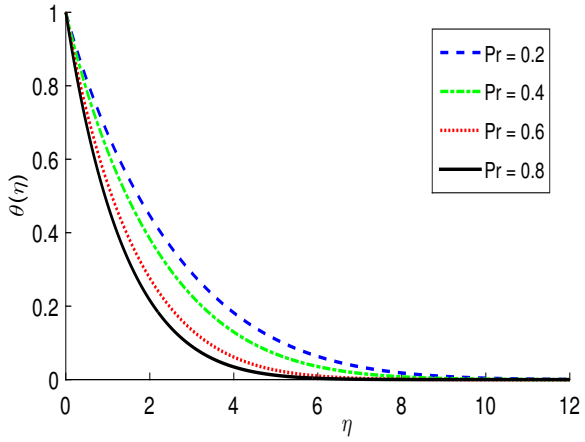

FIGURE 4.1: $\theta(\eta)$ for increasing values of Prandtl number.

The Figure 4.1 shows the influence of the Prandtl number (Pr) on the temperature profile ($\theta(\eta)$) is demonstrated for Pr values ranging from 0.2 to 0.8. As Pr increases, thermal diffusivity decreases because Pr is inversely related to thermal diffusivity and directly related to the viscous diffusion rate. This results in a lower thermal diffusion rate, leading to a significant drop in fluid temperature. Additionally, higher Pr values cause a reduction in the thermal boundary layer thickness, indicating a steeper temperature gradient near the surface.

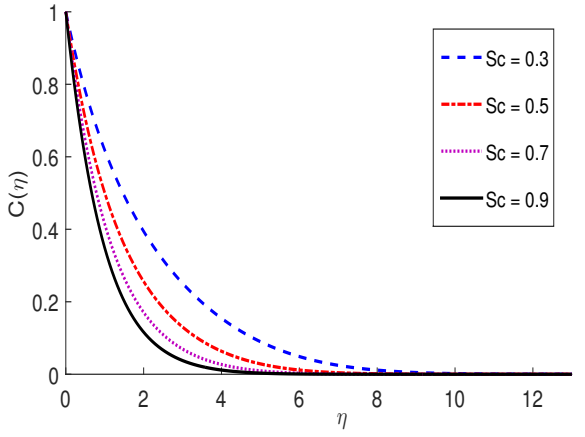

FIGURE 4.2: Concentration profile for various values of Sc.

The Figure 4.2 illustrates the relationship between the dimensionless concentration profile $C(\eta)$ for various values of Schmidt number S_c. As the Schmidt number increases, corresponding to smaller molecular diffusivity, the thermal boundary layer becomes thinner. This results in significant changes in the concentration distribution within the boundary layer, which can be observed from the figure.

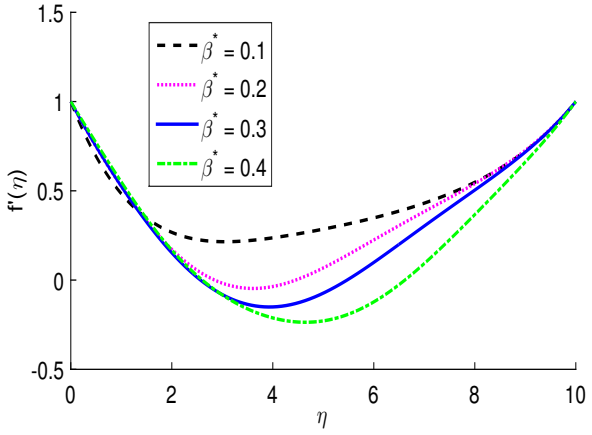

FIGURE 4.3: Hydrodynamic velocity boundary layer profile with increasing micropolar coupling parameter.

Figure 4.3 shows the variation of the hydrodynamic velocity boundary layer profile $f(\eta)$ with increasing micropolar coupling parameter β^*. As β^* increases from 0.1 to 0.4, the velocity profile exhibits a more pronounced decline near the wall and reaches lower minimum values before recovering. This behavior indicates that micropolar coupling enhances the resistance within the boundary layer, leading to a thicker velocity boundary layer and a delayed recovery to the free-stream velocity.

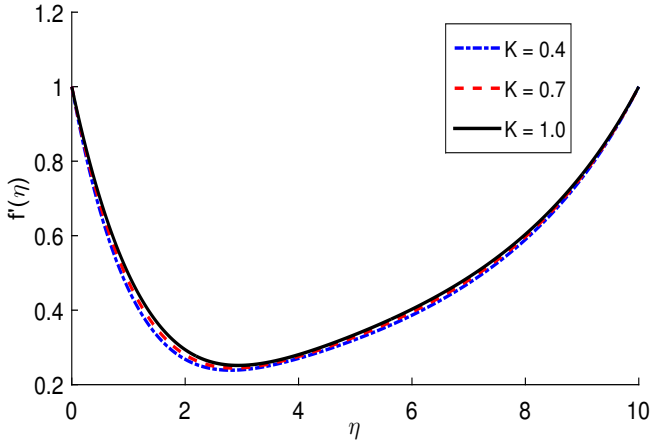

FIGURE 4.4: Hydrodynamic velocity boundary layer profile with increasing values of micropolar parameter K.

The Figure 4.4 illustrates the impact of K on the velocity profile $f'(\eta)$. As K increases, the fluid velocity increases. This can be explained by the physical principles of fluid dynamics: an increase in K leads to a decrease in density, which

reduces the resistance to fluid particle movement. Consequently, the fluid velocity rises more rapidly, as shown in the figure.

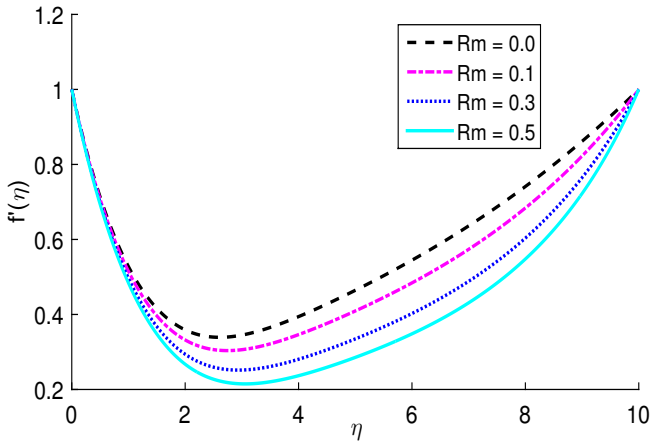

FIGURE 4.5: Hydrodynamic velocity boundary layer profile with increasing magnetic Reynolds number.

Figure 4.5 demonstrates the influence of the magnetic Reynolds number R_m on the velocity distribution. In the absence of magnetic induction effects (i.e., for low R_m), the velocity boundary layer is thinner and exhibits lower peak values. However, as R_m increases, the induced magnetic field enhances the Lorentz force, resulting in a thicker boundary layer and elevated velocity profiles.

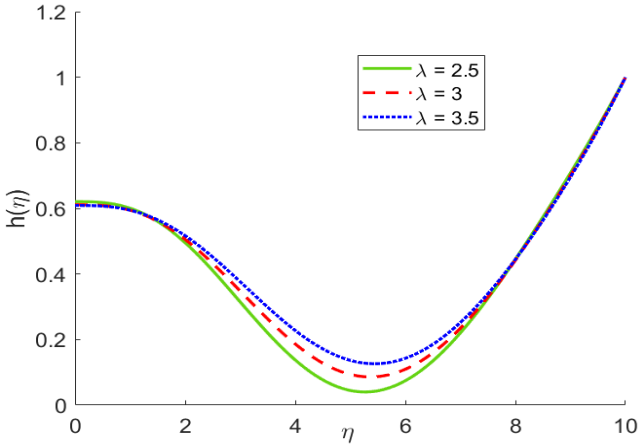

FIGURE 4.6: Magnetic induction profile for various values of magnetization parameter.

Figure 4.6 illustrates the variation of the magnetic induction profile $h(\eta)$ for different values of the magnetization parameter λ. As λ increases, the fluid exhibits

stronger magnetic responsiveness, resulting in a higher magnetic induction across the boundary layer. The dip in $h(\eta)$ becomes shallower, indicating reduced magnetic diffusion. Physically, this reflects the enhanced alignment of magnetic particles with the applied field, highlighting the stabilizing role of magnetization in magnetohydrodynamic flows.

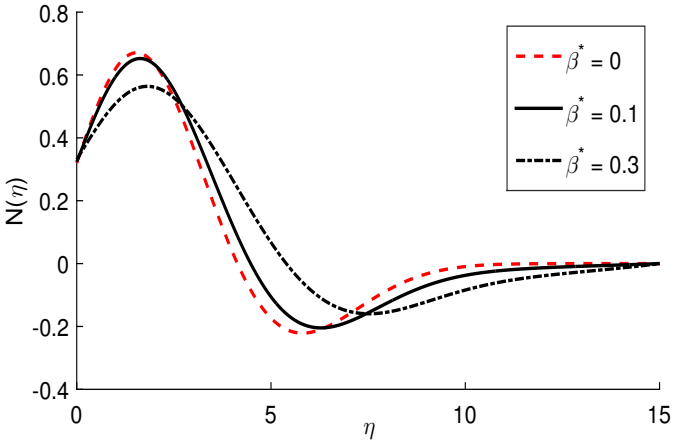

FIGURE 4.7: Micro-rotational velocity profile for increasing micropolar coupling parameter.

Figure 4.7 shows the variation of the micro-rotational velocity profile $N(\eta)$ with increasing micropolar coupling parameter β^*.

The profile exhibits a peak followed by oscillatory decay as η increases. As β^* increases from 0 to 0.3, the peak magnitude of $N(\eta)$ decreases, and the oscillations dampen more rapidly, indicating that higher micro-inertial coupling suppresses microrotational motion and enhances flow stabilization.

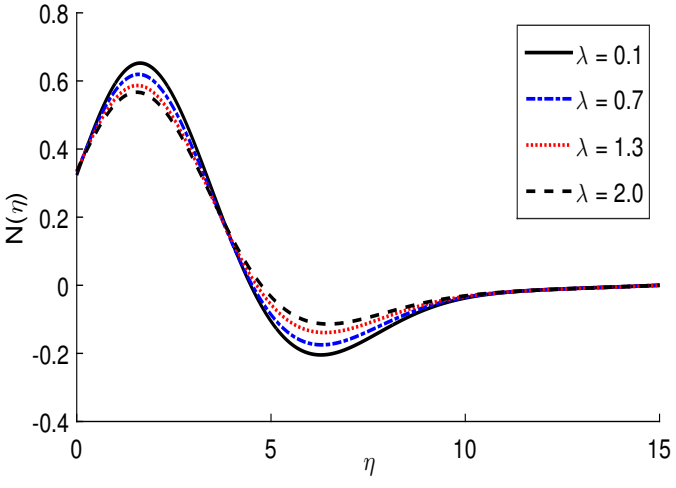

FIGURE 4.8: Micro-rotational velocity propfile for magnetization parameter λ.

Figure 4.8 illustrates the effect of the magnetization parameter on the micro-rotational velocity. Lower values of the parameter λ lead to a decrease in micro-rotational velocity, while higher values of λ result in an increase in micro-rotational velocity.

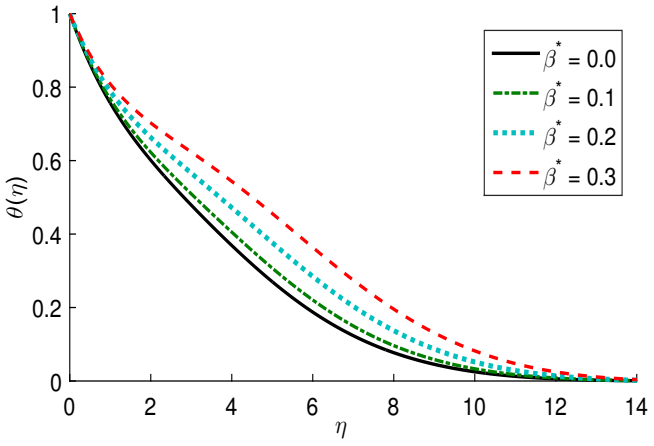

FIGURE 4.9: Temprature profile for increasing values of micropolar coupling parameter β^*.

In Figure 4.9, the parameter β^* influences the microscopic flow of the fluid and its interaction with thermal behavior, depending on the fluid's microstructural features. The influence of β^* on the temperature profile is evident in the figure. It is clear that as β^* increases, the temperature profile also increases.

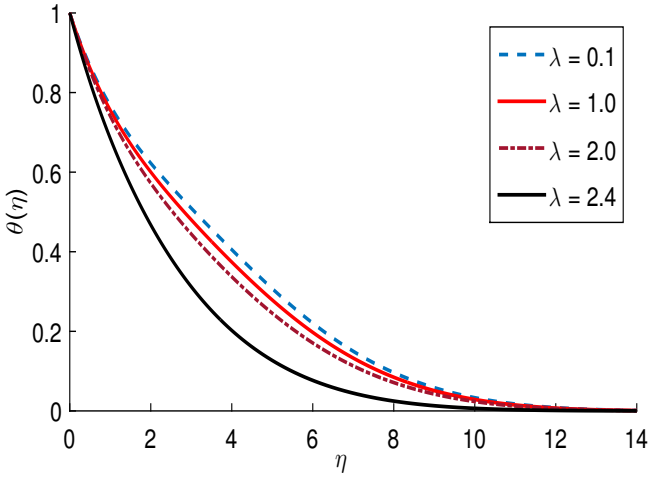

FIGURE 4.10: Temprature profile for increasing λ.

In Figure 4.10, the fluid temperature decreases with increasing values of the magnetization parameter. This indicates that higher values enhance the rotational

effects in the fluid, which in turn promote greater heat dissipation, leading to a reduction in temperature.

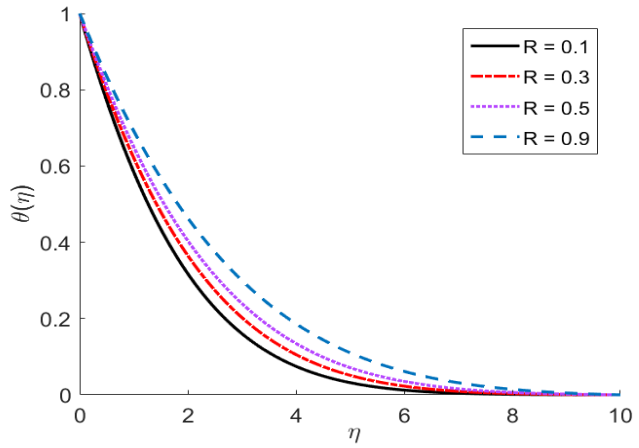

FIGURE 4.11: Temprature profile for increasing values of Radiation parameter.

The Figure 4.11 shows the impact of the radiation parameter on the temperature profile. In this graph, it is observed that as the value of the radiation parameter increases, the temperature profile $\theta(\eta)$ also increases. Consequently, the rate of heat transfer decreases with an increase in the radiation parameter because the temperature profile increases.

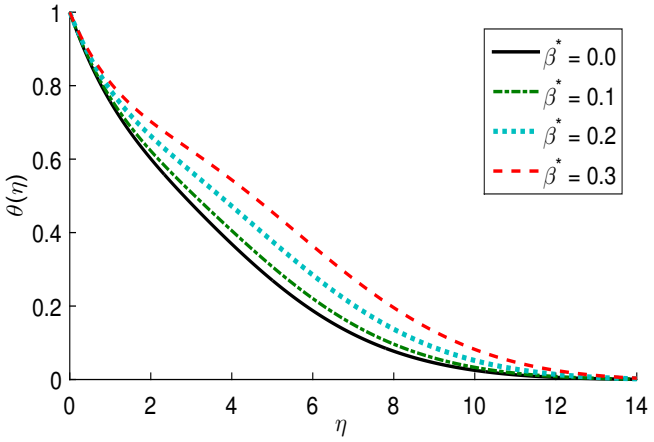

FIGURE 4.12: Temperature profile $\theta(\eta)$ for varying β^*.

In Figure 4.12,the temperature profile $\theta(\eta)$ exhibits an increasing trend as the value of the Micropolar coupling parameter β^* increases. This indicates that higher values of β^* enhance the thermal energy within the system, leading to an overall rise in temperature. The physical interpretation of this behavior suggests that the

micromagnetic and rotational effects contribute to increased thermal conduction or energy dissipation, thereby elevating the temperature distribution across the domain.

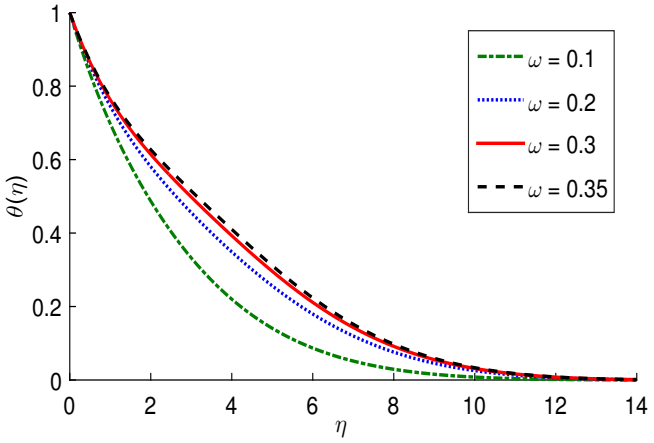

FIGURE 4.13: Temperature profile $\theta(\eta)$ for varying ω.

Figure 4.13 illustrates the influence of the parameter ω on the temperature profile. The observed results suggest that an increase in ω leads to a corresponding rise in the temperature profile. As ω increases, a noticeable upward shift in the temperature distribution is observed, highlighting the significant effect of this parameter on the thermal characteristics of the system.

Tables 4.1, and 4.2 present the numerical values of the Nusselt number $-\theta'(0)$, and Sherwood number $-\phi'(0)$, respectively, for varying values of key physical parameters. These dimensionless quantities offer valuable insights into the fluid's behavior in terms of momentum, heat, and mass transfer near the boundary layer. The parameters varied include the MMR parameter ω, the micropolar coupling parameter β^*, the magnetization parameter λ, and the micropolar parameter K. A detailed analysis of the influence of these parameters on each of the dimensionless quantities is provided below.

The Nusselt number, denoted by $-\theta'(0)$, quantifies the convective heat transfer rate at the surface. A higher value signifies more efficient heat transfer from the surface to the fluid. As ω increases, the Nusselt number shows a decreasing trend, signifying that rotation has a dampening effect on heat transfer. For instance, when ω increases from 0 to 0.3 (with $\beta^* = 0.1$), the Nusselt number decreases from 0.5207 to 0.4300. This reduction can be attributed to the thickening of the thermal

TABLE 4.1: Nusselt number $-\theta'(0)$ for varying physical parameters.

S No.	ω	β^*	λ	K	$-\theta'(0)$
1	0	0.1	0.5	1	0.52074908
2	0.1	0.1	0.5	1	0.52714704
3	0.25	0.1	0.5	1	0.438419868
4	0.3	0.1	0.5	1	0.430016096
5	0	0.15	0.5	1	0.508154169
6	0.1	0.15	0.5	1	0.516629094
7	0.3	0.15	0.5	1	0.416206789

TABLE 4.2: Sherwood number $-\phi'(0)$ for varying physical parameters.

S No.	ω	β^*	λ	K	$-\phi'(0)$
1	0	0.1	0.5	1	0.69835578
2	0.1	0.1	0.5	1	0.70465461
3	0.25	0.1	0.5	1	0.617258888
4	0.3	0.1	0.5	1	0.607311057
5	0	0.15	0.5	1	0.688791453
6	0.1	0.15	0.5	1	0.697032751
7	0.3	0.15	0.5	1	0.59211686

boundary layer due to rotational forces, which impede the convective transport of heat. An increase in β^* from 0.1 to 0.15 also leads to a slight decrease in the Nusselt number, indicating that micropolar effects may hinder thermal conduction within the fluid. The presence of micro-rotations likely disrupts the temperature gradients near the wall, reducing heat transfer efficiency.

The Sherwood number $-\phi'(0)$ characterizes the rate of mass transfer at the surface, analogous to the Nusselt number for heat transfer. A higher Sherwood number indicates more efficient mass transfer. Similar to heat transfer, the mass transfer rate decreases with increasing rotation. As ω rises from 0 to 0.3 (with $\beta^* = 0.1$), the Sherwood number drops from 0.6983 to 0.6073. This indicates that rotation leads to the thickening of the concentration boundary layer, which inhibits the diffusion of species away from the surface. Furthermore, increasing β^* from 0.1 to 0.15 leads to a moderate decrease in the Sherwood number. This suggests that micropolar effects, similar to their impact on heat transfer, inhibit mass diffusion near the wall due to the disturbance of concentration gradients by micro-rotational fluid elements. This detailed analysis offers a comprehensive understanding of how the interplay of MMR, micropolarity, and other parameters influences the fundamental transport phenomena in boundary layer flows.

Chapter 5

Conclusions and Future Work

In conclusion, this thesis extends the model developed by Khan and Hameed [9], which focused on heat transfer in magnetohydrodynamic (MHD) micropolar flow. Our study investigates the effect of micromagnetorotation (MMR) on the concentration in chemically reacting processes within the micropolar boundary layer. The analysis demonstrates the impact of different concentration and energy-related parameters on velocity, temperature, and concentration distributions, as well as on skin friction. By transforming the governing nonlinear partial differential equations (PDEs) into dimensionless ordinary differential equations (ODEs) through similarity transformations, we obtained numerical solutions using the shooting method. The results were then analyzed and presented graphically, emphasizing the significant effects of key parameters on the velocity, temperature, and concentration profiles.
The main findings are summarized as follows

- An increase in the Prandtl number leads to a reduction in the thermal boundary layer thickness.
- As the Schmidt number increases, the concentration boundary layer thickness decreases.
- With increase in the magnetic Reynolds number the fluid velocity also increases.

- An increase in the radiation parameter leads to a corresponding increase in the thermal boundary layer thickness.
- Increase in β^* leads to increase in the velocity and temperature boundary layer thickness.
- The magnetic induction profile exhibits a rising trend with an increase in the magnetization parameter.
- The micro-rotational velocity profile increases with an increase in the magnetization parameter.

In the future, this investigation can be extended with rates effect in chemical reaction equation. Some other important physical aspects for instance, viscous dissipation, bioconvection and micropolar effects can be incorporated in the presented model. Moreover, this model can be utilized to study the boundary layer flows with thermal slip and thermal convective boundary conditions.

Bibliography

[1] A.C Eringen. Theory of micropolar fluids. *Journal of mathematics and Mechanics*, pages 1–18, 1966.

[2] T. Ariman, M.A Turk, and N.D Sylvester. Microcontinuum fluid mechanics—a review. *International Journal of Engineering Science*, 11(8):905–930, 1973.

[3] K. Shizawa and T. Tanahashi. New constitutive equations for conducting magnetic fluids with internal rotation: thermodynamical discussions. *Bulletin of JSME*, 29(255):2878–2884, 1986.

[4] A.C. Eringen. *Microcontinuum field theories: I. Foundations and solids*. Springer Science & Business Media, 2012.

[5] J.V. Ramana Reddy, V. Sugunamma, and N. Sandeep. Simultaneous impacts of joule heating and variable heat source/sink on mhd 3d flow of carreau-nanoliquids with temperature dependent viscosity. *Nonlinear Engineering*, 8 (1):356–367, 2019.

[6] E.G. Karvelas, N.K. Lampropoulos, T.E. Karakasidis, and I.E. Sarris. Blood flow and diameter effect in the navigation process of magnetic nanocarriers inside the carotid artery. *Computer Methods and Programs in Biomedicine*, 221:106916, 2022.

[7] M. Saraswathy, D. Prakash, and P. Durgaprasad. Mhd micropolar fluid in a porous channel provoked by viscous dissipation and non-linear thermal radiation: an analytical approach. *Mathematics*, 11(1):183, 2022.

[8] M. Almakki, H. Mondal, and P. Sibanda. Onset of unsteady mhd micropolar nanofluid flow with entropy generation. *International Journal of Ambient Energy*, 43(1):4356–4369, 2022.

[9] M.S. Khan and I. Hameed. A new magneto-micropolar boundary layer model for liquid flows–effect of micromagnetorotation (mmr). *arXiv preprint arXiv:2308.08457*, 2023.

[10] A. Tulu. Analysis of magnetohydrodynamic micropolar nanofluid flow due to radially stretchable rotating disk employing spectral method. *Advances in Mathematical Physics*, 2023(1):5283475, 2023.

[11] P.V.S. Narayana, B. Venkateswarlu, and S. Venkataramana. Effects of hall current and radiation absorption on mhd micropolar fluid in a rotating system. *Ain Shams Engineering Journal*, 4(4):843–854, 2013.

[12] M.A. Kumar, Y.D. Reddy, B.S. Goud, and V.S. Rao. International journal of thermofluids. 2020.

[13] M.S. Khan, M.A. Memon, I. Khan, and S.M. Eldin. Finite element based direct and iterative approach to investigate a magneto-micropolar flow through a rectangular channel. *Alexandria Engineering Journal*, 75:55–66, 2023.

[14] M.A.A. Mahmoud. Thermal radiation effects on mhd flow of a micropolar fluid over a stretching surface with variable thermal conductivity. *Physica A: Statistical Mechanics and its Applications*, 375(2):401–410, 2007.

[15] D. Srinivasacharya and U. Mendu. Free convection in mhd micropolar fluid with radiation and chemical reaction effects. *Chemical Industry and Chemical Engineering Quarterly*, 20(2):183–195, 2014.

[16] M. Sagheer, M.S. Khan, S. Khatoon, and H. Shahzad. A numerical study of boundary layer flow of a magneto-micropolar fluid affected by micromagnetorotation. *Physica Scripta*, 2025.

[17] R.W. Fox, A.T. McDonald, and P.J. Pitchard. Introduction to fluid mechanics, 2004, 2006.

[18] R.K. Bansal. *A textbook of fluid mechanics*. Firewall Media, 2005.

[19] J.N. Reddy and D.K. Gartling. *The finite element method in heat transfer and fluid dynamics*. CRC press, 2010.

[20] J. Ahmed and M.S. Rahman. Handbook of food process design.

[21] F. Mabood, S. Shateyi, M.M. Rashidi, E. Momoniat, and N.J.A.P.T. Freidoonimehr. Mhd stagnation point flow heat and mass transfer of nanofluids in porous medium with radiation, viscous dissipation and chemical reaction. *Advanced Powder Technology*, 27(2):742–749, 2016.

[22] P.A. Davidson and A. Thess. *Magnetohydrodynamics*, volume 418. Springer Science & Business Media, 2002.

[23] M. Gad-el Hak. *Frontiers in experimental fluid mechanics*, volume 46. Springer Science & Business Media, 2013.

[24] R.W. Lewis, P. Nithiarasu, and K.N. Seetharamu. *Fundamentals of the finite element method for heat and fluid flow*. John Wiley & Sons, 2004.

[25] J. Kunes. *Dimensionless Physical Quantities in Science and Engineering*. Elsevier, 2012.